

An experimental dynamic study of cement mortar with polyurethane residues and foundry sand



Lucas Ramon Roque da Silva ^{a,*}, Flávio Cirino Gaspar Junior ^b, Paulo Cesar Gonçalves ^c, Valquíria Claret dos Santos ^c, Mirian de Lourdes Noronha Motta Melo ^a, Guilherme Ferreira Gomes ^a

^a Mechanical Engineering Institute, Federal University of Itajubá, Brazil

^b Institute of Production Engineering and Management, Federal University of Itajubá, Brazil

^c Institute of Physics and Chemistry (IFQ), Federal University of Itajubá, Brazil

ARTICLE INFO

Keywords:

Artificial Neural Network
Exhaust foundry sand
Modal Responses
Mortar
Polyurethane
Response Surface Methodology

ABSTRACT

Although many studies have reported on the application of experimental, statistical, numerical, and computational tools to composite structures, few have focused on the use of analysis of variance (ANOVA) to analyze experimental data and Artificial Neural Network (ANN) as a technique to predict the modal responses of Portland cement mortars. In this study, by means of DOE and ANN the modal responses of portland cement mortars with polyurethane waste and foundation sand from exhaustion were investigated. The tests were performed by means of free vibration and the analyzed responses were natural frequency and damping factor. The experimental results indicated that the combined PU and FES waste can significantly change the natural frequency and damping of the mortars. This change, when compared to the reference samples, can reach an increase of 11.6% or decrease of 21.7%, depending on the percentage of waste used. The ANN trained with the experimental data showed a high correlation to predict the experimental results.

1. Introduction

One of the biggest challenges for civil engineering today is the production of high-performance materials without producing significant waste or that incorporate recycling materials in their composition. However, in the last decades the target of the production of materials was only the performance, thus the environmental issue related to the waste of its production was neglected. This has resulted in the rampant production of waste of various kinds such as plastics, wood, cement, for example, in the last decade were produced approximately 1.00 and 1.13 billion tons of construction waste in the U.S. and China, respectively [52].

Therefore, research that aims to performance characteristics of materials and at the same time use recycled materials is important. This study was based on this premise, the wastes explored in this study are polyurethane (PU) and exhaust casting sand (FES) which are of different physical and chemical nature but which impact the environment in an equivalently negative way [55]). The foundry sand, on the other hand, is a by-product of metallurgical production, the so-called function sand or

green sand is incorporated into molds that can be reused several times during the production of metal parts [50,51]. During part manufacturing, factory exhaust fans capture high surface area sand residue that comes loose in the molds. FES is the airborne residue that comes loose from molds and can be captured by exhaust fans. Thus, FES is generally finer than conventional exhaust sand [64]. And because it is thinner, its disposal in the environment is difficult due to the numerous possibilities of contamination to the local fauna and flora [65]. The PU originates from the polymer family, so it is very versatile and can come in many shapes and sizes and be used on a large industrial scale [20]. This product has a low production cost and high durability, and is widely used in the construction sector and in the household appliance trade in general [12,62].

One of the characteristics that need to be studied in cementitious mortars and concrete are the dynamic properties, or how this type of material behaves under dynamic loading. In this way, modal analysis is a technique for examining the dynamic properties of structures. Modal analysis is often performed by computer analysis and experimental modal analysis (EMA) in this way it is able to distinguish vibration modes, natural frequencies and damping rate [35].

* Corresponding author at: Federal University of Itajubá, 1303, Avenue BPS, Itajubá, Brazil.

E-mail address: d2020101800@unifei.edu.br (L. Ramon Roque da Silva).

Nomenclature

ANN	Artificial neural network
ANOVA	Analysis of variance
DOE	Design of experiments
FES	exhaust casting sand
FFT	Fast Fourier transform
FRF	Frequency response function
GFFD	General full factorial design
MPUFES	Mortar With Polyurethane and Exhaust Foundation Sand
PU	Polyurethane
RSM	Response surface methodology
S/C	Sand by cement
SC	Coarse Sand Ratio
U _{max}	maximum displacement
x ₁	factor
x ₂	factor
y	Response variable
β	Model constant
ΔE	lost energy
η	Loss factor or loss coefficient
ω _r	Resonance frequencies or natural frequency

Some recycled materials have natural advantages regarding mechanical energy dissipation and high damping rates. One of these characteristics is the presence of a weak ITZ that decreases the friction and sliding behavior between each internal of the material [81–34]. Another characteristic is uniform particle size distribution and compact form factor that can provide better vibration energy distribution. Finally another characteristic is the low specific mass and large voids that provide better vibration energy dissipation [75].

The very good damping characteristic of cementitious materials using waste shows the potential for application of this environmentally friendly material in structural vibration control [44]), for instance, on the basis of subway or high-speed trains [36,71]. Nevertheless, the implementation of these technologies to achieve better vibration control still requires a progress on two key problems: a better energy-efficient concrete and a process to build the gap between the damping properties of concrete materials and their elements and structures [37].

Reinforced concrete structures that are made of cementitious materials are inevitably subjected to dynamic loads. These loads may be part of their use and occupation such as vehicular traffic on a bridge, pedestrians walking along a walkway or stairway. Other loads that are significant, such as wind, earthquakes, and explosions that vary in intensity during the life of a building and cause dynamic responses in the structure [23]. Damping is an essential parameter for determining the dynamic response of a structure under various possible loads and determining the degree of damage before low to medium intensity events occur [67]. It is widely accepted that damping represents the energy dissipation capability of a material or structure. However, due to the complex nature and mechanisms of multiple responses, modeling damping behavior is still an active area of study [37].

The reason that damping behaviors cannot properly be explained by a unique universal damping model is that the damping of concrete materials is composed mainly of viscoelastic damping and hysteresis damping (Clarence W. [15]). For concrete materials, both the viscoelastic damping model and the complex damping model are widely used in assessing their viscous damping [31]. For concrete materials, the viscous damping model that considers the energy dissipated by various sources is commonly applied in structural design and analysis, and the equal viscous damping ratio is used to depict the damping capacity of concrete structures [22]. For the majority of cases, it is reasonable and acceptable

to apply viscous damping and the associated equivalent viscous damping ratio in describing the internal damping characteristics of the concrete material and structure [32].

The incorporation of alternative materials with high damping properties, such as polymers, has been considered to promote the energy dissipation capacity of cementitious materials. This is done by considering their high flexibility and viscous damping mechanism [18]). Since the 1990 s research has been done related to the topic. [19]) are the first ones to discover the behavior of rubberized concrete, and they have found that it exhibited lower compressive and tensile strength than natural coarse aggregate due to the low modulus and high Poisson's ratio of rubber. In addition, the incorporation of rubber crumb varied the failure characteristics from brittle to ductile and plastic failure. Subsequently [72,27;68] performed research with results similar to those found by Eldin and Senouci [19]. A study seeking the optimization and improvement of the damping properties of concrete with polymeric materials was performed by [58], in which analyzed the final microstructure of the material.

Compared with the natural aggregate, the dynamic performance of concrete gets significant improvement with the incorporation of polymeric nature products, contrary to what happens with the mechanical performance. [77] found results of 60 % improvement in 20 % of substitution, [49] 35 % in 30 % of substitution, [83] that this improvement can reach up to 140 % in 45 % of substitution. The equivalent viscous damping ratio of concrete columns (columns) with rubber obtained 13 % and 150 % improvement in dissipation energy [80].

The research related to concrete damping with cementitious materials is still in its early stages. But with the results already achieved it is safe to say that the incorporation of polymeric materials can improve the damping performance, flexibility and energy dissipation of cement elements [33]. According to [35], the improvement of damping can happen through a correct combination of coarse aggregate, fine aggregate, and polymeric material.

Regarding the dynamic properties, not only concrete with polymeric waste but also waste of various natures have been researched as a partial substitute for natural aggregates. [40 82] conducted reverse cyclic stress tests on beam-column connections and found that as the axial compression ratio increases, both the energy consumption and ductility decrease substantially. Using recycled concrete blocks [16] demonstrated that the building structure fully complies with seismic fortification standards using simulated vibration of the structure. [57] performed creep tests, loading and unloading tests, and free vibration tests on reinforced RAC beams of varying ages and found that the damping characteristic of the RAC is related to the instantaneous recoverable deformation. Concrete with recycled aggregate structure's basic mode shape has a lower natural frequency and a higher damping ratio than the concrete with natural aggregate structure [76 74]. Studying the damping ratio of reinforced concrete structures Japan, [69] identifies substantial damping ranges that can be achieved by structures. An evaluation of the seismic resistance capacity of concrete with recycled material was performed by [41] and proved that it has resistance. In this study the author calculated an average equivalent viscous damping value of 0.217 at the ultimate load cycle using a low cycle load test on a recycled concrete column with a size ratio of 1:2.5. [38] investigated the seismic performance of concrete with recycled concrete columns after freeze-thaw cycles. The experimental results indicate that at the same displacement level, the equivalent viscous damping coefficient of concrete with recycled column aggregate is slightly increased. [34] found that the frequency of vibration of concrete is log-normal and that the damping ratio distribution is a superposition of two log-normal distributions. They measured the damping of recycled concrete using the free vibration dampening method. [81] determined the dynamic modulus and nonlinear damping characteristics of concrete with recycled aggregate, as well as the static compressive strength and modulus of elasticity of concrete with recycled aggregate, using cyclic uniaxial compression experiments their results indicated that concrete with recycled

aggregate had a higher loss factor than concrete with natural aggregate.

The use of artificial neural network in cementitious materials has been explored to predict behavior in terms of mechanical strength, chemical reactivity and physical properties. Author [8] makes the prediction of mortar strength based on its mixing components through artificial neural networks. The highly nonlinear relationship between the compressive strength of the mortar and the mixed components makes it difficult to predict strength. The study presents maps of compression resistance in order to facilitate the sizing of the mortar mixture.

Use of artificial neural network (ANN) to predict the compressive and flexural strength of a mortar made with modified zeolite additive (MZA) [53]. The input data used were six parameters: amount of cement, amount of silica sand, amount of modified zeolite additive (MZA), amount of water, curing period and load weights. The output data consisted of the compressive or flexural strength. The author concludes that ANN can be used to predict experimental results related to compressive and flexural strength.

Study the natural hydrated lime mortar and through a database uses three degrees of hydration, different aggregates and water content is performed by [7]. Artificial neural networks are used to describe the influence of mortar design on compressive strength. The study reveals that neural networks are effective in predicting the influence of input parameters used at different hydration ages.

Use of artificial neural network in corrosion modeling in cementitious mortars by the author [39]. It is known that many of the factors that affect corrosion are difficult to control. Thus, the artificial neural network can be a technique to be considered due to its ability to tolerate relatively imprecise, noisy or incomplete data, lower vulnerability to outliers, filtering capacity and adaptability. The study generates a corrosion current density prediction model using the artificial neural network approach. Several variables were used as input variables, namely: age, water/cement ratio, cement content, compressive strength, and type of kneading water, corrosion potential, solution resistance and polarization resistance. Finally, the resulting neural network model satisfactorily predicted the corrosion current density.

Based on the studies described, it is evident that the use of ANN to predict the behavior of cementitious materials is promising. Thus, the use of ANN to predict dynamic properties of mortars is justifiable. The authors highlight this as an innovation or novelty promoted by the present study.

In this study, the natural fine aggregate of Portland cement mortar was replaced by the combination of PU and FES to achieve the best configuration of energy dissipation capacity and damping properties. Thus, PU and FES were considered as partial substitutes for natural sand and the modifications of these variables were investigated. Other variables investigated were sand/cement S/C ratio and coarse sand SC content in the variation of properties. In this way, it is sought to produce an ecological mortar with relatively low cement consumption and reuse of natural resources. The modal data (natural frequency and loss factor) obtained from modal testing data were submitted to analysis of variance in order to evaluate its statistical significance. A design of experiments was performed considering a Response surface methodology (RSM) to obtain the best cement mortar manufacturing parameters. Finally, an artificial neural network is constructed to predict the modal properties based on manufacturing factors. Finally, the best designs from both methods were compared.

2. Theoretical background

2.1. Structural vibration

Modal analysis can be defined as the study of the dynamic characteristics of a system independently of the applied loads and the respective responses of the structure or system. Thus the modal analysis identifies different modes of frequency, damping and deformation

specific to each structure or system (P.[54]).

The modal analysis consists of evaluating the dynamic characteristics of a structure or system. These dynamic characteristics are known as modal shapes, damping, and natural frequency. According to the conditions of use/operation, structures are subjected to dynamic and/or static loads at the same time. That will respond to the excitations and the response must be quantified and analyzed within the defined design conditions. The observations of dynamic responses as a whole do not provide enough information to understand the structure or the system behavior, the modal analysis is configured as the best way to interpret the dynamic behavior of a structure [42].

According to the conditions of use/operation, structures are subjected to dynamic and/or static loads at the same time. That will respond to the excitations and the response must be quantified and analyzed within the defined design conditions. The observations of dynamic responses as a whole do not provide enough information to understand the structure or the system behavior, the modal analysis is configured as the best way to interpret the dynamic behavior of a structure [29,59].

Natural frequency is the frequency at which a system will vibrate by itself, without external forces, after an initial perturbation. The number of natural frequencies of a system or structure can be obtained by the number of degrees of freedom of that system or structure. The vibration modes, on the other hand, are the deformations that each component should present when vibrating at its natural frequency. The decrease in oscillation of a system occurs due to the phenomenon of damping, which can be measured by the coefficient ζ , called damping ratio, which describes how oscillations decay after a disturbance [61].

The occurrence of damping results in energy loss from a system and the most common use for quantifying energy loss is the loss factor coefficient, denoted by η . The loss factor represents the lost energy (ΔE) by the potential energy at maximum displacement (U_{\max}) [11] which is given in Equation (1). It is worth noting that when resonance occurs the loss factor is equal to twice the damping ratio.

$$\eta = \frac{\Delta E}{2\pi U_{\max}} \quad (1)$$

There are two widespread ways of measuring modal analysis is that using an accelerometer or a laser vibrometer. Using an accelerometer, you get acceleration data over time. And using a vibrometer gives velocity data over time. In order to calculate the frequency response function (FRF) the fast Fourier transform (FFT) is used, in which it is possible to transform the data over time into the frequency domain. The frequency response function can be understood as the ratio between the output response of the structure and the applied load that caused the response. Due to the use of the FFT, the FRF has both real and imaginary components. Phase and magnitude components can also be obtained and provide useful information for obtaining the dynamic parameters [84].

By detecting the peaks in the magnitude plot of FRF one can obtain the natural frequencies. These peaks are confirmed as resonant frequencies ω_r by observing a 180° variation in the phase plot at the same frequency value as the peak. The local maxima are used to determine two points ('a' and 'b') called the half power points, obtained by dividing the response value by $\sqrt{2}$. After obtaining the half power points, the loss factor η_r of this particular mode can be estimated by Equation (2) [63].

$$\eta_r = \frac{\omega_a^2 - \omega_b^2}{2\omega_r^2} \quad (2)$$

In a multiple degrees of freedom system, the method called Least-squares time is commonly used [26]. In which it consists of using a curve-fitting algorithm to obtain the modal parameters, Equation (3)[x(t)] describes the free vibration response of a system with multiple degrees of freedom.

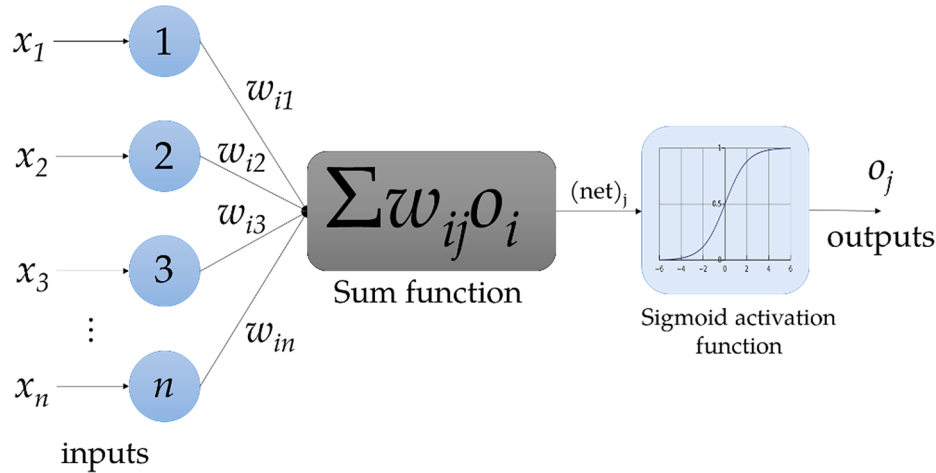


Fig. 1. The artificial neuron model (adapted from (Saridemir, 2009).

$$x(t) = \sum_{i=1}^N e^{-\eta_i t} \cdot [a_i \cdot \sin(\omega_{di} t) + b_i \cdot \cos(\omega_{di} t)] \quad (3)$$

The coefficients a_i and b_i describe the vibration amplitude, ω_{di} represents the damped natural frequency and η_i refers to the damping ratio. By fitting the experimentally obtained response by Equation (3) [$x(t)$] it is possible to identify all the modal parameters [61].

In this study, the vibration responses were obtained using a vibrometer to acquire the data and velocity over time. In this way the FRF was processed by an FFT. To obtain the structural modal response results, the natural frequencies were extracted considering the peak-to-peak method and the structural damping value (loss factor), extracted by the model curve fitting method.

2.2. Artificial neural networks

Artificial neural networks (ANN) theory was first published in 1940 by McCulloch and Pitts, and has since been developed and has begun to acquire importance as technology advances [30]. ANN is designed in about the same way that the human brain is, with simple circuits connected by artificial neurons. The synapses formed by the connections formed between neurons are responsible for conveying impulses and distributing information, and are commonly used in learning algorithms

[14]. The ANN approach has the capability of learning from data set training experience. After the training, the ANN should be able to detect output replies based on unknown input data, making it a useful tool for a variety of applications [28].

The ANN approach has the capability of learning from data set training experience. After the training, the ANN should be able to detect output replies based on unknown input data, making it a useful tool for a variety of applications [17,78]. Weights describe the inhibitory or excitatory action of neural connections, which might be negative or positive depending on whether the connections are inhibitory or excitatory. The weight of the relevant connection ($X_i \times W_i$) is multiplied by the value (intensity) of the received signal to compute the influence of a signal received from another neuron. The total of all $X_i \times W_i$ connections' values is added together, and the result is sent to the activation function [60]. The activation function describes how a node or nodes in a network layer convert the weighted sum of the input into an output [60].

The interaction between data and an ANN is governed by learning paradigms. Unsupervised learning and supervised learning are the two basic types of learning paradigms [21]. In supervised learning, the network is given instances and the response is compared to the desired answer. The error signal, which is the difference between the two responses, is used to change the synaptic weights in the network. This

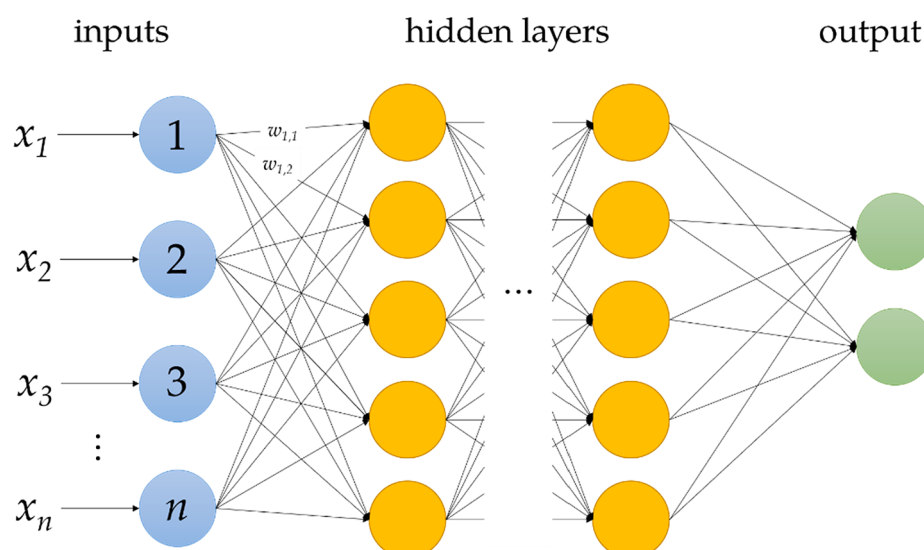


Fig. 2. Feedforward Neural Network.

process is repeated until the network responds statistically adequately. Because the method in unsupervised learning does not strive to know the intended outputs, it does not use instances of input and output to be learned by the network. The self-organization of the ANN [60].

In addition, neural networks are classified according to how they propagate information, which can be either a feed-forward or a back-propagation network. Information flows in just one direction in feed-forward networks; that is, it flows from the input layer to the output layer in only one direction [70]. Information can travel back and forth between layers in backpropagation networks [13]. For an adequate ANN configuration, you should design a model that is not too stiff to not correctly describe the data, but also not too flexible to model the data's noise.

All perceptron-solvable issues can be resolved with just one hidden layer, however there are situations when using two or three hidden layers is more effective. The network's predictions for the outside environment are then produced by the neurons in the output layer (Sardemir, 2009). A typical neural network is depicted in Fig. 1 with input, output, sum function, and sigmoid activation function. The output of the linked neuron is multiplied by the synaptic strength of the connection between them to determine the input to a neuron from another neuron. Using Equation (4), the weighted sums of the input components (net_j) are computed.

$$(\text{net})_j = \sum_{i=1}^n w_{ij} o_i + b \quad (4)$$

Where $(\text{net})_j$ is the weighted sum of the j^{th} neuron for the input received from the preceding layer with n neurons, w_{ij} is the weight between the j^{th} neuron in the preceding layer, o_i is the output of the i^{th} neuron in the preceding layer. The network input (net_j) and the neuron's output signal (o_j in Fig. 1) are connected by a transformation function known as the activation function. Ramp, sigmoid, and Gaussian functions are the most often used activation functions. In general, for multilayer receptive models as the activation function $f(\text{net}_j)$ sigmoid function is used. The output of the j^{th} neuron o_j is calculated by using Equation (4) with a sigmoid function as shown in Equation (5).

$$o_j = f(\text{net})_j = \frac{1}{1 + e^{-\alpha(\text{net})_j}} \quad (5)$$

Where α is constant that regulates how steeply the semi-linear region slopes. With the exception of the input layer, every layer has the sigmoid nonlinearity active. The outputs (0,1) of the sigmoid function described by Equation (5).

A network of neurons dispersed over three or more layers makes up the feedforward multilayer perceptron network (ANN) (see Fig. 2). Although there are no connections between neurons in the same layer, every neuron in each of these layers is entirely connected to every neuron in the layer above it and the one below it. The input layer, also known as the ANN input parameters, is the initial layer and has the same number of neurons as inputs. The last is the output layer i.e. the "results" of the ANN, with the same number of neurons as problem outputs. The layer or layers between these two are known as the hidden layers. The number of hidden layers and the number of neurons in each hidden layer depend on the problem under study and cannot be known beforehand [1].

3. Experimental methodology

3.1. General full factorial design

The systematic method called Design of experiments (DOE) is used to determine the relationship between factors that affect a process and its results [56]. Usually, the DOE method can be divided into full factorial design (FFD) and fractional factorial design also known as Taguchi Experimental Design (TED). In FFD design, all combinations of the

Table 1
Input factors and their levels.

Control variables	Abbreviation	Symbol	Level	
Sand by cement	S/C	X ₁	1	3
Coarse Sand Ratio	SC	X ₂	20 %	50 %
Foundry Exhaust Sand	FES	X ₃	10 %	40 %
Polyurethane	PU	X ₄	0 % 10 %	30 % 60 %

Table 2
Physical properties of fine and coarse aggregates.

Properties	Cement	Lime	NS	PU	FES
Density (kg/m ³)	3140	1600	2650	660	2700
Specific surface (m ² /kg)	330	–	5	20	29.4
Initial setting time (min)	120	–	–	–	–
Final setting time (min)	500	–	–	–	–
Water absorption (%)	–	–	0.95	0.05	0.75
Unit Weight (kg/m ³)	1440	1120	1350	220	1450

parameter levels are tested in order to analyze the results. The so-called General full factorial design (GFFD) is a variation of FFD, which allows running more than two levels per variable [79]. The variables and their ranges are given in Table 1. In the GFFD setup there are 3 levels with 4 control factors S/C, CS, FES, and PU. The tests were performed in triplicate for each mixture, the software used for the analyses was Minitab version 2018.

The Table 2 shows the characterization of the materials used to prepare the mortar.

In Table 1, S/C represents two families of 1:1 to 1:3 (read, one parts binder to three parts sand) mixtures, with the binder consisting of cement plus hydrated lime in the ratio of 4:1, i.e., four parts cement and one part lime. The CS denotes the percentage of coarse sand replacing fine sand from 20 % to 50 %, where the coarse sand has a granulometry ranging from 1.2 mm to 4.8 mm and the fine sand from 0.75 mm to 1.2 mm; the mass of FES replaces NS from 10 % to 40 %; the mass of PU replaces NS from 0 %, 10 %, 30 % to 60 %. The water to cement ratio (w/c) in the 1:1 mix was equal to 0.45 and for the 1:3 mixtures it was 0.60. The superplasticizer content was 1.0 of the cement weight for all mixtures. With these proportions were obtained spreads in the fresh state of 260 ± 25 mm recommended by the standard [2] for coating mortar use that was taken as the limit for control of the study.

With these proportions, measures of fresh state spreading of 260 ± 50 mm were obtained, close to that recommended by the standard [2] for the use of coating mortar, which was taken as the limit for the study control. A standard deviation of ± 50 mm was allowed because, some combinations of proportions obtained facilitated spreading and others hindered by the incorporation of FES and PU waste. As the focus of this study is only on dynamic properties, we fixed this range for study so that we could compare the groups without changing w/b ratio and/or %S_p.

By means of the experimental arrangement chosen in the GFFD with 3 variables of 2 levels and 1 variable of 4 levels, the number of 32 mixtures of MPUFS was reached. For the mixtures, three replicates were performed in order to increase the reliability of the results. Thus, a total of 96 samples of MPUFS were tested for the complete development of the GFFD and, consequently, the generation of the ANN. MATLAB software version 2019 was used to run and analyze the ANN.

The Table 3 shows all mixtures with the decoded units and consumption of all materials per mixture. The notations used in this Table 3 (M₁, M₂, ..., M_n) represent the mixtures and their respective number in the numbering sequence. Although the experiments appear in the Table 3 in ascending order, they were performed in a random order in the laboratory to avoid possible biases. The mixtures M_{R1}, M_{R2}, M_{R3}, M_{R4} represent the reference mixtures without incorporation of FES and PU residues.

Table 3Uncoded units and consumption of materials by m³.

Mixtures code	SC	S/C	FES	PU	Cement(g)	Lime(g)	NS(g)	FES(g)	PU(g)	Sp(g)	w/c
M ₁	20 %	1	10 %	0 %	786.62	196.66	707.96	78.7	0.00	7.87	0.45
M ₂	20 %	1	10 %	10 %	786.62	196.66	688.16	78.7	19.80	7.87	0.45
M ₃	20 %	1	10 %	30 %	786.62	196.66	648.56	78.7	59.40	7.87	0.45
M ₄	20 %	1	10 %	60 %	786.62	196.66	589.17	78.7	118.80	7.87	0.45
M ₅	20 %	1	40 %	0 %	786.62	196.66	471.97	314.6	0.00	7.87	0.45
M ₆	20 %	1	40 %	10 %	786.62	196.66	452.18	314.6	19.80	7.87	0.45
M ₇	20 %	1	40 %	30 %	786.62	196.66	412.58	314.6	59.40	7.87	0.45
M ₈	20 %	1	40 %	60 %	786.62	196.66	353.18	314.6	118.80	7.87	0.45
M ₉	20 %	3	10 %	0 %	455.70	113.92	1321.52	45.6	0.00	4.56	0.60
M ₁₀	20 %	3	10 %	10 %	455.70	113.92	1287.11	45.6	34.41	4.56	0.60
M ₁₁	20 %	3	10 %	30 %	455.70	113.92	1218.30	45.6	103.23	4.56	0.60
M ₁₂	20 %	3	10 %	60 %	455.70	113.92	1115.07	45.6	206.46	4.56	0.60
M ₁₃	20 %	3	40 %	0 %	455.70	113.92	1184.81	182.3	0.00	4.56	0.60
M ₁₄	20 %	3	40 %	10 %	455.70	113.92	1150.41	182.3	34.41	4.56	0.60
M ₁₅	20 %	3	40 %	30 %	455.70	113.92	1081.59	182.3	103.23	4.56	0.60
M ₁₆	20 %	3	40 %	60 %	455.70	113.92	978.36	182.3	206.46	4.56	0.60
M ₁₇	50 %	1	10 %	0 %	786.62	196.66	707.96	78.7	0.00	7.87	0.45
M ₁₈	50 %	1	10 %	10 %	786.62	196.66	688.16	78.7	19.80	7.87	0.45
M ₁₉	50 %	1	10 %	30 %	786.62	196.66	648.56	78.7	59.40	7.87	0.45
M ₂₀	50 %	1	10 %	60 %	786.62	196.66	589.17	78.7	118.80	7.87	0.45
M ₂₁	50 %	1	40 %	0 %	786.62	196.66	471.97	314.6	0.00	7.87	0.45
M ₂₂	50 %	1	40 %	10 %	786.62	196.66	452.18	314.6	19.80	7.87	0.45
M ₂₃	50 %	1	40 %	30 %	786.62	196.66	412.58	314.6	59.40	7.87	0.45
M ₂₄	50 %	1	40 %	60 %	786.62	196.66	353.18	314.6	118.80	7.87	0.45
M ₂₅	50 %	3	10 %	0 %	455.70	113.92	1321.52	45.6	0.00	4.56	0.60
M ₂₆	50 %	3	10 %	10 %	455.70	113.92	1287.11	45.6	34.41	4.56	0.60
M ₂₇	50 %	3	10 %	30 %	455.70	113.92	1218.30	45.6	103.23	4.56	0.60
M ₂₈	50 %	3	10 %	60 %	455.70	113.92	1115.07	45.6	206.46	4.56	0.60
M ₂₉	50 %	3	40 %	0 %	455.70	113.92	1184.81	182.3	0.00	4.56	0.60
M ₃₀	50 %	3	40 %	10 %	455.70	113.92	1150.41	182.3	34.41	4.56	0.60
M ₃₁	50 %	3	40 %	30 %	455.70	113.92	1081.59	182.3	103.23	4.56	0.60
M ₃₂	50 %	3	40 %	60 %	455.70	113.92	978.36	182.3	206.46	4.56	0.60
M _{R1}	20 %	1	0 %	0 %	786.62	196.66	786.62	0.00	0.00	7.87	0.45
M _{R2}	20 %	3	0 %	0 %	455.70	113.92	1367.09	0.00	0.00	4.56	0.60
M _{R3}	50 %	1	0 %	0 %	786.62	196.66	786.62	0.00	0.00	7.87	0.45
M _{R4}	50 %	3	0 %	0 %	455.70	113.92	1367.09	0.00	0.00	4.56	0.60

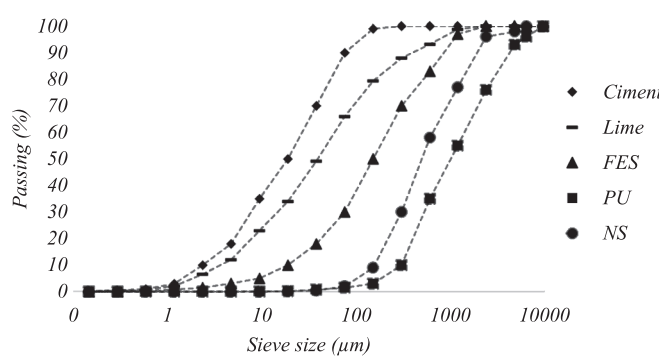


Fig. 3. Particle size distribution.

3.2. Manufacturing and materials

The materials used in this study were: cement type CP II-E-32 [3], hydrated lime [5] as binders, natural sand (NS), foundry exhaust sand (FES), polyurethane powder (PU) as aggregate.

The FES has a predominant composition of SiO₂, Fe₂O₃ which was obtained by X-ray fluorescence analysis. The PU has a predominant composition of C, H, O, N, respectively which was obtained by infrared spectroscopy analysis. The Fig. 3 represents the particle distribution of the binder (cement and lime), obtained by the laser ray diffraction method and aggregates (NS, FES, PU) obtained by sieving on the normal sieve series, [4][25]. Potable water was used for molding and curing the samples. Furthermore, according to [9], 1.5 % of water reducing admixture, 3rd generation superplasticizer based on modified synthetic carboxylated polymers with specific weight of 1.24 kg/lit) was used to

increase the consistency of the MPUFS with the lowest possible (w/b) ratio.

In the current study, FES and PU were used as fine aggregate and replaced the NS in mass in different percentages. The PU used comes from the recycling of household appliances, more specifically from domestic refrigerators; it was obtained through a donation from the company Industria Fox®. The recycling process used by Industria Fox® consists first of filtering the refrigeration gases Chlorofluorocarbon (CFC) that contribute to the destruction of the ozone layer, and persistent organic contaminants such as mercury present in the refrigerator compressor. Such gases are treated by a chemical process that transforms the gas into an acid solution, so that it may be used later by the chemical industry. The leftovers of the device are shredded and the remains of plastic, iron, aluminum and any other materials that can be reused are separated and sent to recycling companies and cooperatives (Industrias [24]).

The foundry waste industry produces countless by-products, from used or residual foundry sand, slag, ash, refractories, coagulants, dust from the exhaust system (filters), scrap, vapors and residual kiln liquids [64,73]. In the current study, the FES was obtained through donation from the company Mahle Metal Leve AS®, Itajubá. The FES is a type of foundry sand waste that is generated by mixing sand, bentonite and charcoal in the manufacturing process of green sand molds for casting metal parts. During the release of the parts by vibratory transport, the very fine sand particles that remain in suspension are filtered through bag filters [43]. It is necessary to remove FES from the casting process, because due to its powdery size it impairs the permeability of the molds and makes it difficult for the process gases to escape. With this, bubbles and harmful voids can be formed in the castings [66].

First, the dry materials, cement, aggregates were mixed with two thirds of the total volume of water and then mixed for 2 min. Then the

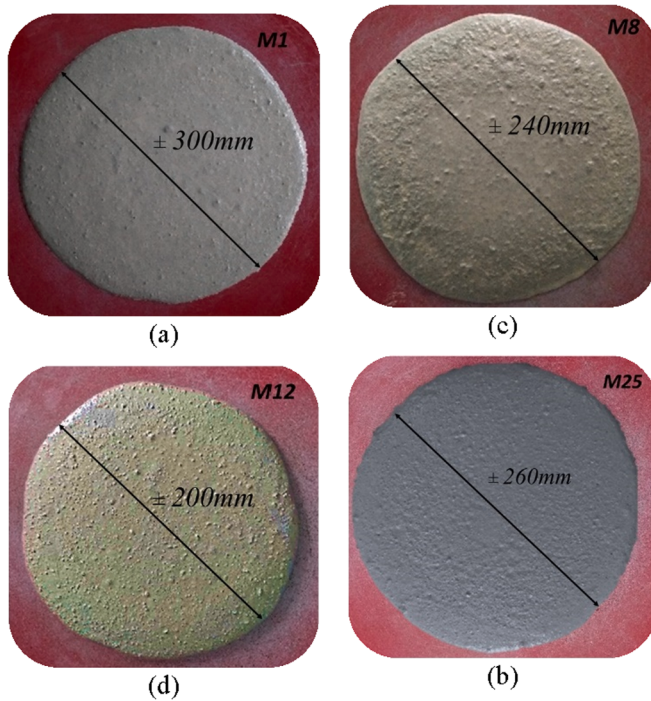


Fig. 4. Spreading test of the MPUFES samples. (a) sample M₁, (b) sample M₈, (c) sample M₁₂, (d) sample M₂₅.

remaining water and the superplasticizer were slowly added and mixed for another 4 min. Next, consistency index test was performed on MPUFS in the fresh state according to the standard [2]. Finally, the fresh MPUFS was placed in the molds for the physical and mechanical tests, respectively. The samples remained in an environment with relative humidity higher than 90 % for 24 h and then were submerged in drinking water in a curing tank with saturated lime water at $21 \pm 3^{\circ}\text{C}$.

The first two tests that were performed were the voids content and absorption by immersion, according to the prescriptions of [6], for mortar with 28 days of age, using specimens with 50 mm in diameter and 100 mm in height. Three samples were molded for each mortar mixture developed.

The mortars tested in the spreading test are shown in Fig. 4. All mortars had a slump range of 250 ± 50 mm. The mixtures in the Fig. 4

were carefully chosen among the various mixtures produced in this study, because they represent well how some visual changes occurred in the fresh state. It is worth noting that the study does not intend to analyze the fresh state characteristics of the mortar, but the authors found it worthwhile to represent the change of physical aspect that occurred in the mixtures during the incorporation of waste and the change of some parameters such as S/C and w/c content.

3.3. Experimental setup

The MPUFS samples were evaluated for forced vibration tests in which the external force was produced by a shaker (small hammer). The equipment used in the tests is shown in Fig. 5. For the experimental tests were performed considering a free, or unsupported, configuration. For this, metallic cables were used to support the sample during the execution of the shaker impact. The Fig. 5 represents the test setup, in which is formed by a sensor, a vibrator, a data acquisition and signal analysis system, note a metallic support was used for the specimens to reach the free vibration or unsupported condition. The instruments used in the experiment include LabVIEW programming, Data Acquisition board (DAQ), laser sensor and shaker. A DAQ plate used was a Photon + model from Brüel&Kjær. A laser vibrometer, model VQ-500-D from Ometron, was used for measuring the vibration displacement at a targeted point. For the free vibration analysis, an impact hammer, Brüel & Kjær, was used in the modal experimental test. The vibration shaker, model 4808 from Brüel & Kjaer, was triggered by the voltage signal from the power amplifier, model 2712 from Brüel & Kjaer. The RT Pro Photon program was used to process all the signals obtained.

Cementitious products in general have low reflective capacity, so for signal acquisition it was necessary to position a plastic tape to assist in signal capture. As the tape has very low thickness and mass compared to the MPUFS samples, it was considered that its presence did not affect the collection of vibration results. It is worth noting that the laser vibrometer for this type of experiment can be considered more suitable than the accelerometer, since the laser is not influenced by the total mass of the system, thus differences in mass of the samples do not affect the vibration results.

In the present study, the modal properties of the different specimens manufactured designs are carried out by acquiring vibration signals with the help of a laser vibrometer (sensitivity 8000 m/s/mV). The sensor is pointed at the surface of the specimen (with the aid of a reflective tape). The output of the vibrometer is fed into the Brüel & Kjaer Photon + DAQ through a USB chassis where the analog vibration signals are

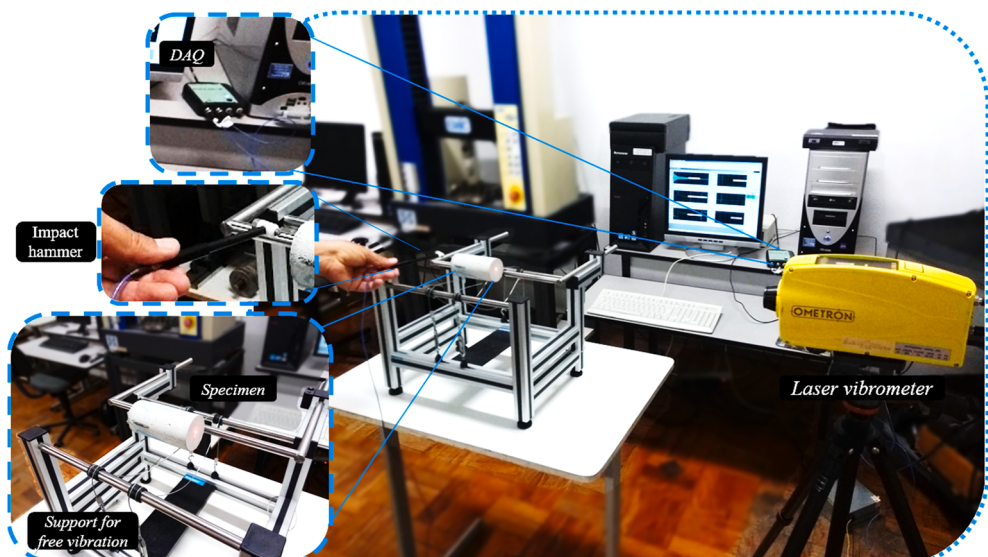


Fig. 5. General experimental setup and details for free vibration.

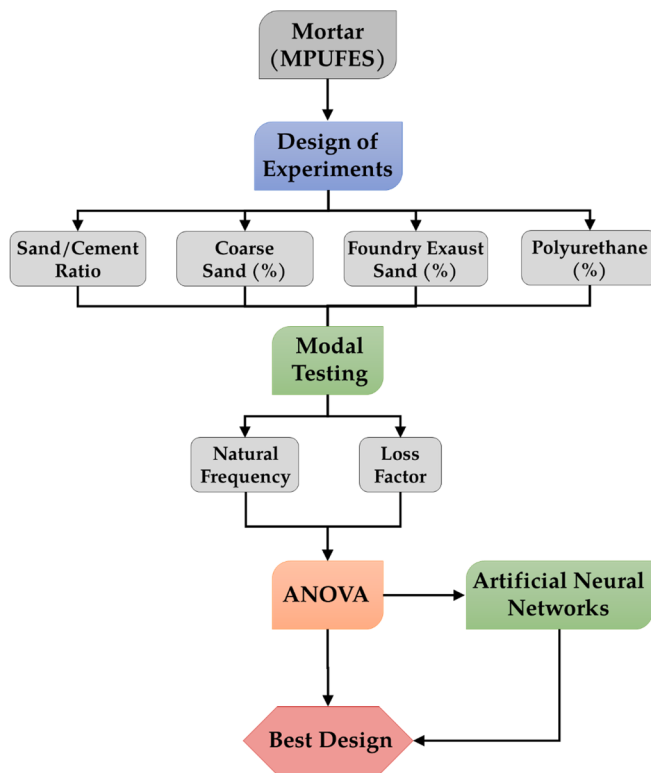


Fig. 6. General flowchart for the full development of the MPUFS study.

conditioned and converted into digital form. The impulse force is applied by using an impact hammer (sensitivity 21.08 m/s²/mV). In order to ensure Shannon's sampling theorem, the sampling frequency was set to 1500 Hz.

The experimental steps of this study have been summarized in Fig. 6. It can be seen that for the production of the MPUFS it was necessary to perform important steps. The first of them is the execution of the General Full Factorial Design of experiments (GFFD), in which a set of variables

was worked on at different levels, which can be seen in Table 1. Then the modal tests were performed and after the analysis of variance, the modeling of the mixing and optimization designs was performed in two ways. One was to use the quadratic model obtained in the RSM-BB configuration used. The other was the use of Artificial Neural Network to arrive at a Modal Properties prediction that will generate a modeling of the mixing projects. This way it will be possible to compare the feasibility of both procedures.

4. Experimental results

In this section, the results obtained by the proposed method are discussed. The first analysis was a free-vibration and forced-vibration analysis, which allowed the responses of residual mortars to be compared with a reference. Statistical results are then evaluated using the RSM and ANOVA methods. Finally, the ANN prediction results are presented.

4.1. Modal results

The first experimental test was for free vibrations using the configuration described in Fig. 5. Free vibration is the response of a system to an initial input, allowing it to vibrate freely. Through it is possible to analyze the natural frequencies and their amplitudes, as well as the damping or loss factor of the system.

Fig. 7 shows the main response of the free vibration time histories of MPUFS composites with all the different design factors tested at the same initial vibration amplitude. The evaluation of the responses obtained in Fig. 7 can be done based on the comparison of the tested material to the adopted benchmark. The damping phenomenon is more pronounced in the samples from M₁₃ to M₁₅ and M₃₀ to M₃₂, in these samples the material presents fast absorption of the oscillation amplitude. In contrast, the samples from the groups M₁ to M₄ and M₁₇ to M₂₀ present low absorption of the oscillation amplitude.

(Intentionally left blank).

Using the Fast Fourier Transform, the damping result expressed in velocity by time is converted into the frequency domain. With the natural frequency of the tested material as a parameter, the Frequency Response Function (FRF), which will offer the initial vibration mode, is

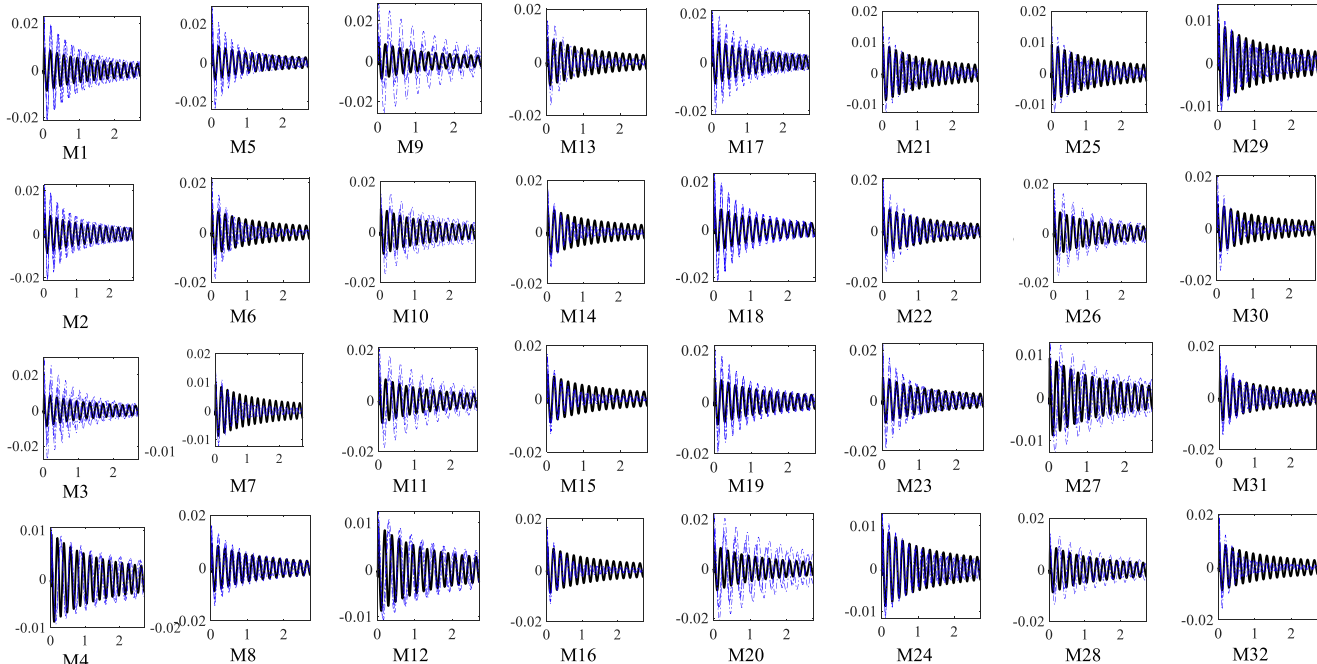


Fig. 7. Velocity time response for considering the different design factors (legend: ■ specimens and ■ reference).

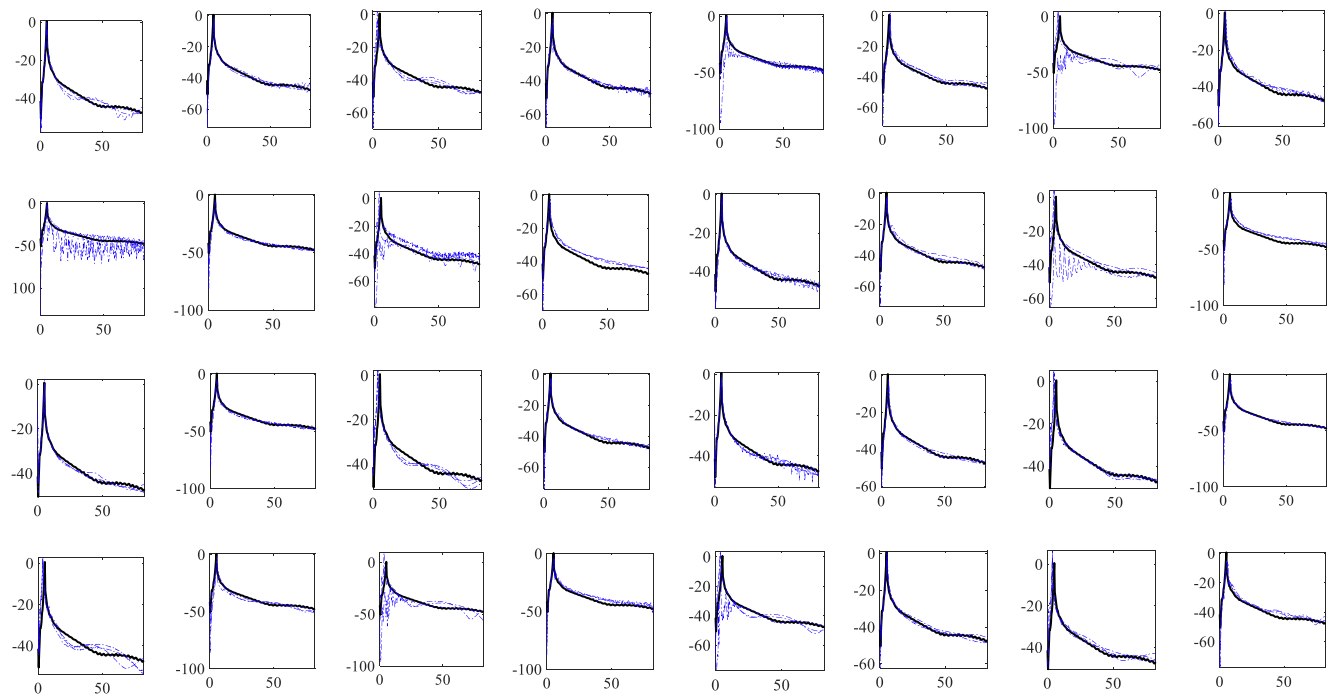


Fig. 8. Frequency response function for considering the different design factors. (legend: ■ specimens and — reference).

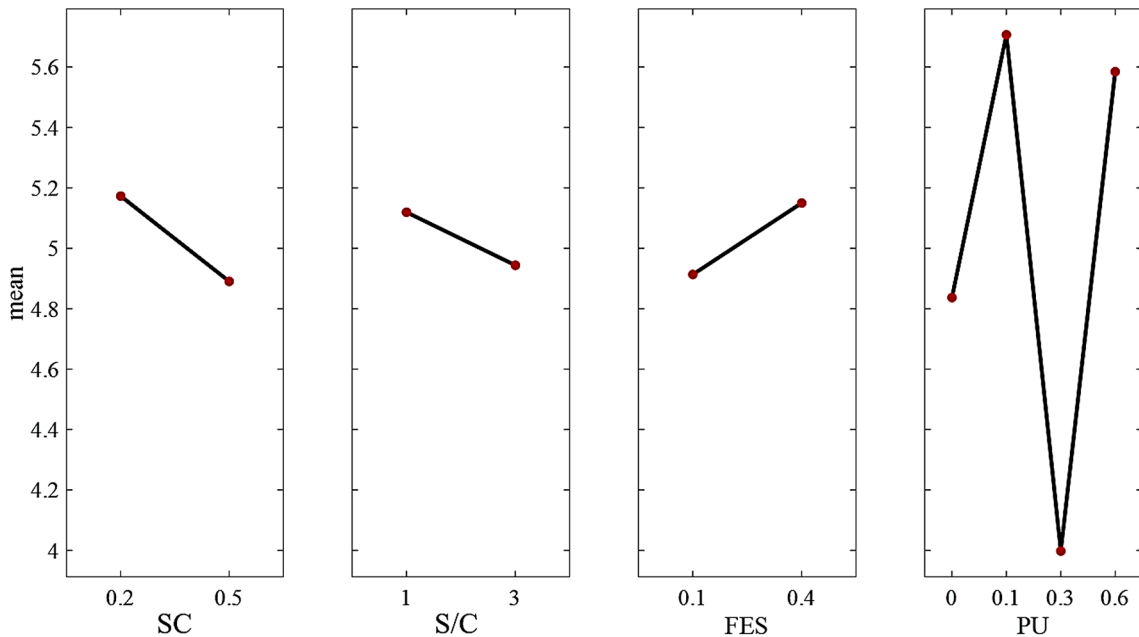


Fig. 9. Main effect plot for the first natural frequency.

generated in this way. In Fig. 8 it is possible to observe that in general the natural frequency of all tested mortars did not change significantly in the first vibration mode or resonant frequency in comparison to the reference sample. The frequency found is close to 5 Hz.

(Intentionally left blank).

4.2. Analysis of variance

The main objective of this research is to dynamically characterize mortars with PU and FES waste incorporation, named as MPUFES. The results were conducted by means of an experimental planning using an RSM, the parameterization was based on four manufacturing factors and

two responses, (see Table 1). The factors were coarse sand content (SC), sand to cement ratio (S/C), replacement content of natural sand with foundry exhaust sand (FES), replacement content of natural sand with polyurethane (PU). The responses were natural frequency and loss factor. Fig. 9 and Fig. 10 represent the results obtained by averaging an analysis of variance (ANOVA) of the responses as a function of the manufacturing factors.

To analyze the statistical results the modal responses were normalized by percentage change analysis, as shown in Equation (6) and Equation (7). The Table 4 summarizes the overall results of this study with the experimental setup and responses.

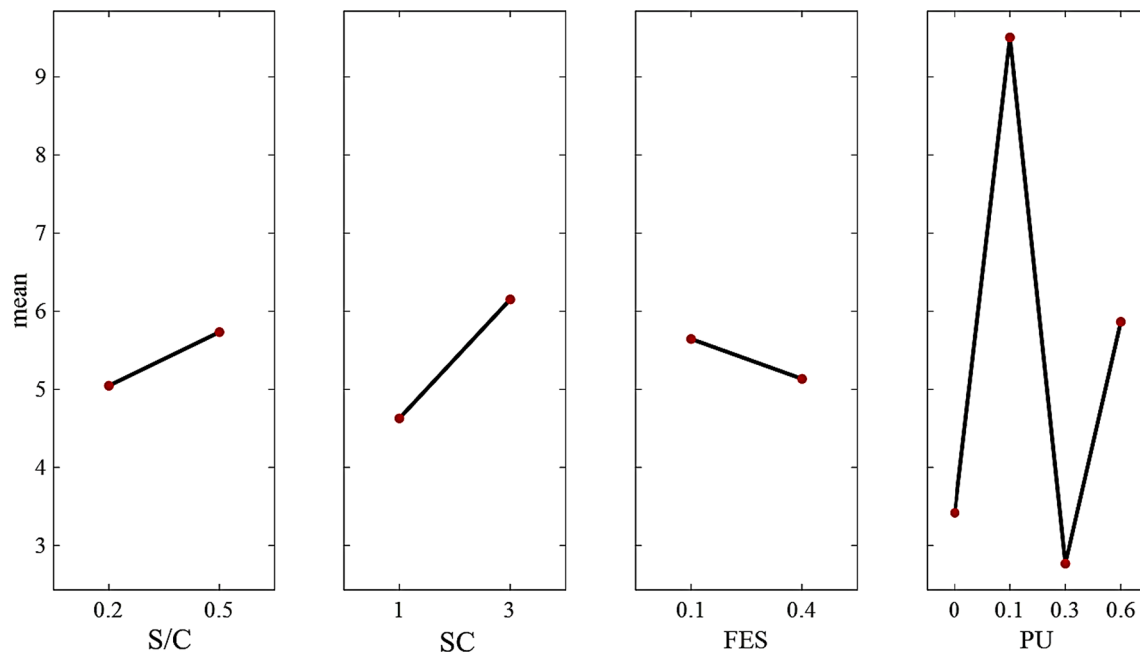


Fig. 10. Main effect plot for the loss factor.

Table 4
Vibrations responses for all the different manufacturing design of MPUFES.

Exp.	Variables				Experimental Responses	
	Coarse Sand (%)	Sand/ Cement	Foundry Ex. Sand (%)	PU	ω_n (Hz)	η (%)
M1	0.2	1	0.10	0.00	5.127	3.280
M2	0.2	1	0.10	0.10	5.493	7.700
M3	0.2	1	0.10	0.30	3.296	4.780
M4	0.2	1	0.10	0.60	5.493	0.070
M5	0.2	1	0.40	0.00	5.127	3.040
M6	0.2	1	0.40	0.10	5.859	3.800
M7	0.2	1	0.40	0.30	9.888	5.000
M8	0.2	1	0.40	0.60	6.226	4.000
M9	0.2	3	0.10	0.00	4.761	6.180
M10	0.2	3	0.10	0.10	6.226	11.580
M11	0.2	3	0.10	0.30	2.930	1.020
M12	0.2	3	0.10	0.60	5.493	10.360
M13	0.2	3	0.40	0.00	5.493	2.920
M14	0.2	3	0.40	0.10	6.226	16.700
M15	0.2	3	0.40	0.30	4.028	1.010
M16	0.2	3	0.40	0.60	5.493	5.500
M17	0.5	1	0.10	0.00	5.127	3.280
M18	0.5	1	0.10	0.10	5.127	7.940
M19	0.5	1	0.10	0.30	3.296	3.390
M20	0.5	1	0.10	0.60	5.859	5.220
M21	0.5	1	0.40	0.00	5.127	3.210
M22	0.5	1	0.40	0.10	5.493	4.880
M23	0.5	1	0.40	0.30	3.662	1.550
M24	0.5	1	0.40	0.60	5.493	5.560
M25	0.5	3	0.10	0.00	3.296	4.040
M26	0.5	3	0.10	0.10	5.859	14.780
M27	0.5	3	0.10	0.30	8.057	5.000
M28	0.5	3	0.10	0.60	5.127	8.000
M29	0.5	3	0.40	0.00	3.662	2.750
M30	0.5	3	0.40	0.10	5.127	13.460
M31	0.5	3	0.40	0.30	3.662	2.300
M32	0.5	3	0.40	0.60	5.859	7.680
M _{R1}	0.2	1	0.00	0.00	5.133	5.090
M _{R2}	0.2	3	0.00	0.00	5.110	5.326
M _{R3}	0.5	1	0.00	0.00	5.055	5.800
M _{R4}	0.5	3	0.00	0.00	5.125	5.051

$$\Delta\omega = \left(1 - \frac{\omega}{\omega_{ref}}\right) \times 100 \quad (6)$$

$$\Delta\eta = \left(1 - \frac{\eta}{\eta_{ref}}\right) \times 100 \quad (7)$$

(Intentionally left blank).

Fig. 9 shows the main effects plot results for the first natural frequency, where for larger sizes, we have smaller values of the natural frequency, while for density, it occurs in the opposite way. A higher value of natural frequency is discovered for greater values. The behavior of the loss factor's primary effects is depicted in Fig. 10. A more in-depth study is challenging in this situation since the size variable does not exhibit a clearly defined pattern. However, for density, we have that the loss factor is higher for higher densities.

The Fig. 9 displays the major impact plot results for the first natural frequency, where lower natural frequency values are observed for larger SC and S/C concentrations. Higher values of natural frequency correspond to higher FES levels. The impact of the PU contents is not well defined; there is no clear pattern within the items that are utilized.

The main impacts plot results for the loss factor are displayed in Fig. 10. Take note of how the tendencies matched those found for the first natural frequency. Naturally occurring frequency values are lower for higher SC and S/C levels. Higher values of natural frequency correspond to higher FES levels. The impact of the PU contents is not well defined; there is no clear pattern within the items that are utilized.

The Interaction plot for the first natural frequency is shown in Fig. 11 and the Interaction plot for the loss factor is shown in Fig. 12. The initial natural frequency and loss factor proportionately are often modified by the researched variables at the various levels tested. The variables are not proportional only in a few limited circumstances. In this instance, SC interacts with PU in a percentage range of 0 % to 10 %.

Integrating the analyses, Fig. 13 displays the response surface combining the two variables, allowing for analysis of their combined effects on natural frequency, loss factor, vibration amplitude, and mass. Natural frequency, loss factor, and amplitude displayed non-linear behavior on the in-space response surfaces, however the mass displayed near-plane (linear) behavior.

In Fig. 13 the combination of analyses represented by means of the response surface was performed. In this scenario it is possible to analyze

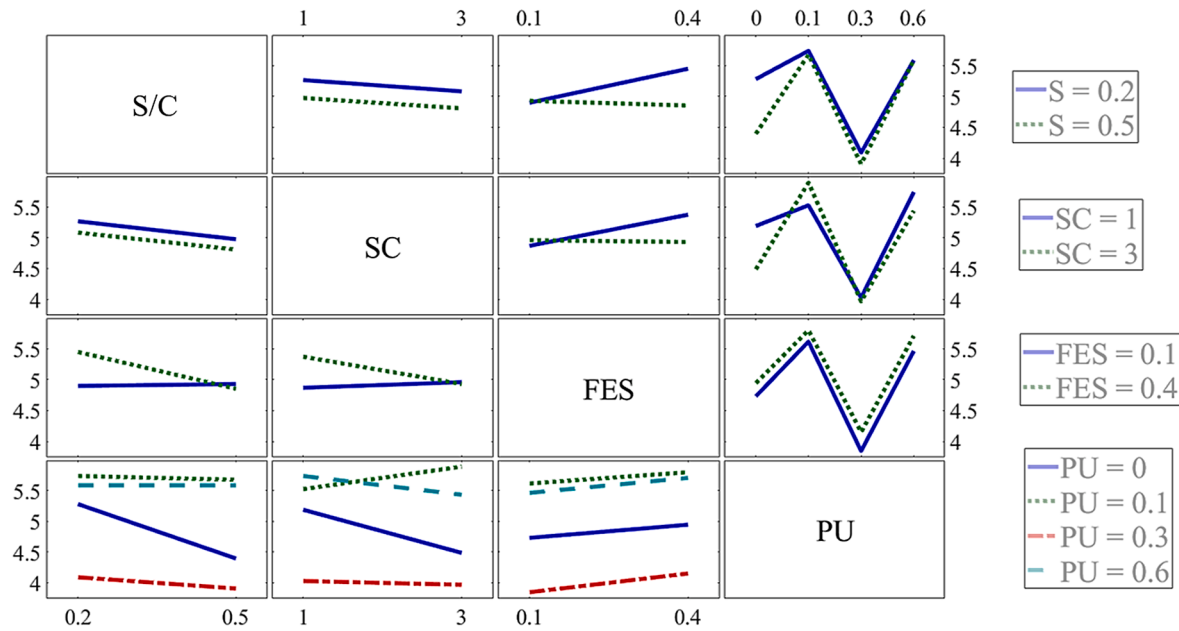


Fig. 11. Interaction plot for the first natural frequency.

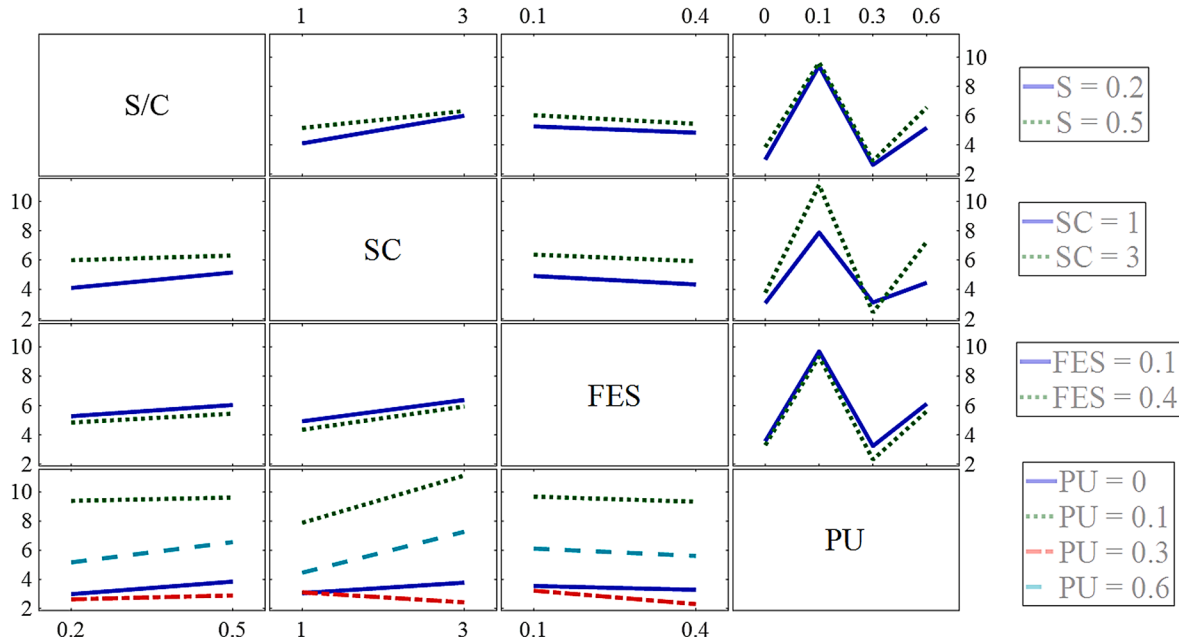


Fig. 12. Interaction plot for the loss factor.

the combination of the effects of the variables on the modal responses tested. Fig. 13a and Fig. 13c behave in a similar manner in which linear behavior occurs. The variables S/C and SC are linear and inversely proportional to ω_n . In Fig. 13a, the maximum value of ω_n occurs for the lowest values of SC and S/C which represents an increase of ω_n by 2.8 % over the average value (reference mixture). In Fig. 13c the pattern is the reverse. For SC and S/C increase, the N increase reaches 27.0 % of the average value.

Fig. 13b the incorporation of PU modifies the ω_n not having a pattern within the analyzed spectrum. However, it can be seen that some points of extreme low and high absolute values occur. This is the case for the percentage of 30 % PU in which the ω_n has a decrease of -27.5 % in relation to the average value. In both Fig. 13c and Fig. 13d, the percentage of 10 % PU causes an increase close to 66.0 % in η , if compared

to the average value (reference mixture). The sharp decrease in natural frequency and loss factor for 30 % polyurethane waste and 0.1 cast exhaust area waste Fig. 13(b) and Fig. 13(d) as it was to be analyzed is directly related to the decrease in loss factor. A low loss factor material represents a material that is able to absorb more impacts in a shorter time interval, i.e., cushion impacts better[10].

(Intentionally left blank).

4.3. Modal properties prediction using ANN

In this section, an ANN was developed to predict the modal responses regarding the modal behavior model of mortars with PU and FES waste. The input layer is composed of design parameters (4 variables) such as coarse sand content (SC), sand to cement ratio (S/C), percentage of FES

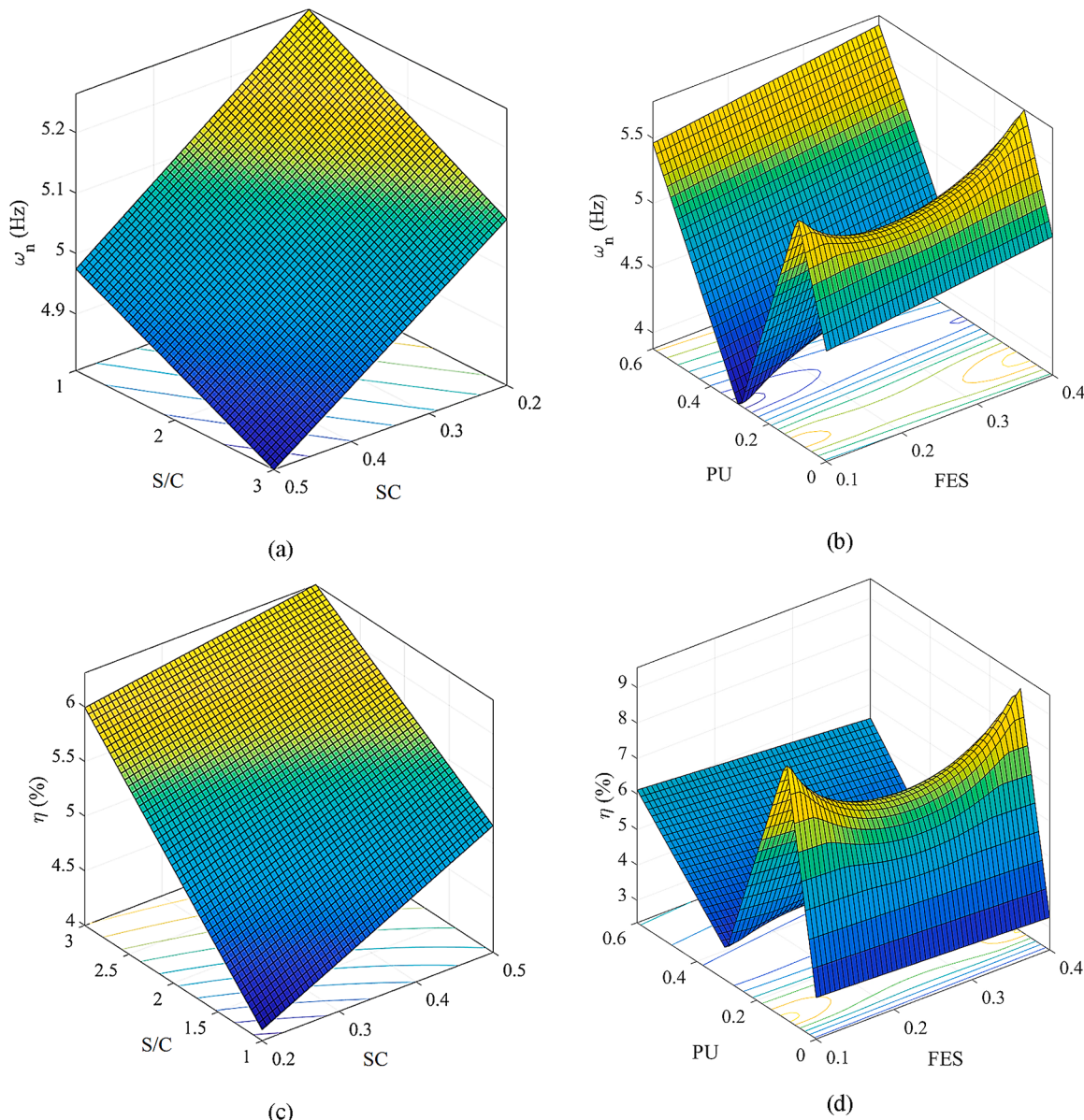


Fig. 13. Response surfaces in the space for (a) ω_n by the variables SC \times S/C; (b) ω_n by the variables PU \times FES, (c) η by the variables SC \times S/C e (d) η by the variables PU \times FES.

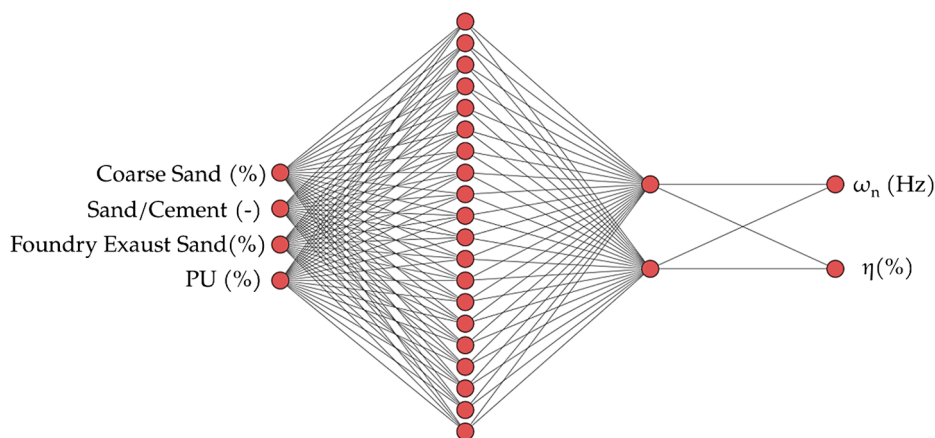


Fig. 14. The architecture used for the ANN.

Table 5

Optimal ANN configuration considering the modal behavior prediction.

Parameters	ANN model for MPUFES
Learning algorithm	Levenberg-Marquardt
Activation function (hidden layers)	Hyperbolic tangent
Activation function (output layers)	Linear
Mean squared error	0.10
Training data	70 %
Max number of iterations	2000
Learning rate	0.30

and percentage of PU replacing natural sand. The output layer is composed of the modal responses of natural frequency, and loss factor or damping rate. Thus, the ANN created has one input layer with four neurons, a hidden layer with 20 neurons and an output layer with 2

neurons, as shown in the architecture of Fig. 14.

The multilayer feedforward network with backpropagation training technique and supervised learning was adopted to obtain high performance. The network is trained using this approach, and the faults it generates are passed down to the previous layers until they are inconsequential (Haykin, 2009). On the ANN architecture, the Levenberg-Marquardt algorithm was utilized to promote a rapid convergence rate and proper training. Table 5 shows the additional parameters employed in the ANN generated here.

In this study, a linear regression analysis was developed in order to verify the correlation between the data sets by ANN for training and validation. The fit is measured by the coefficient of determination (R^2), which has values between $0 \leq R^2 \leq 1$, close to one, the coefficient demonstrates that the variables accurately describe the regression model [45]. As is shown in Fig. 15c, the coefficient of determination was close

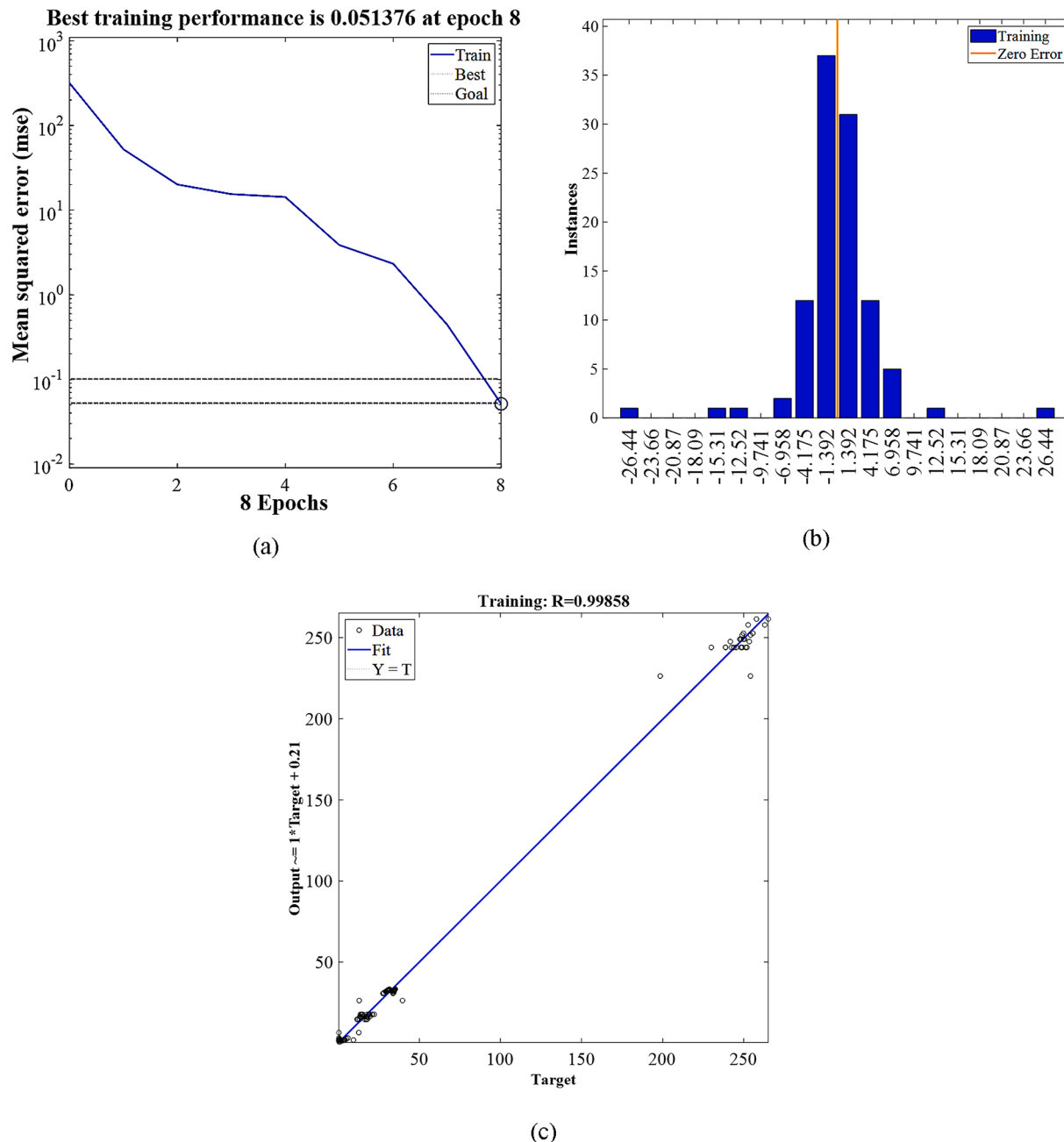


Fig. 15. Results of ANN global training considering: (a) the best training performance, (b) the histogram of error values, and (c) the linear regression analysis with coefficient of determination.

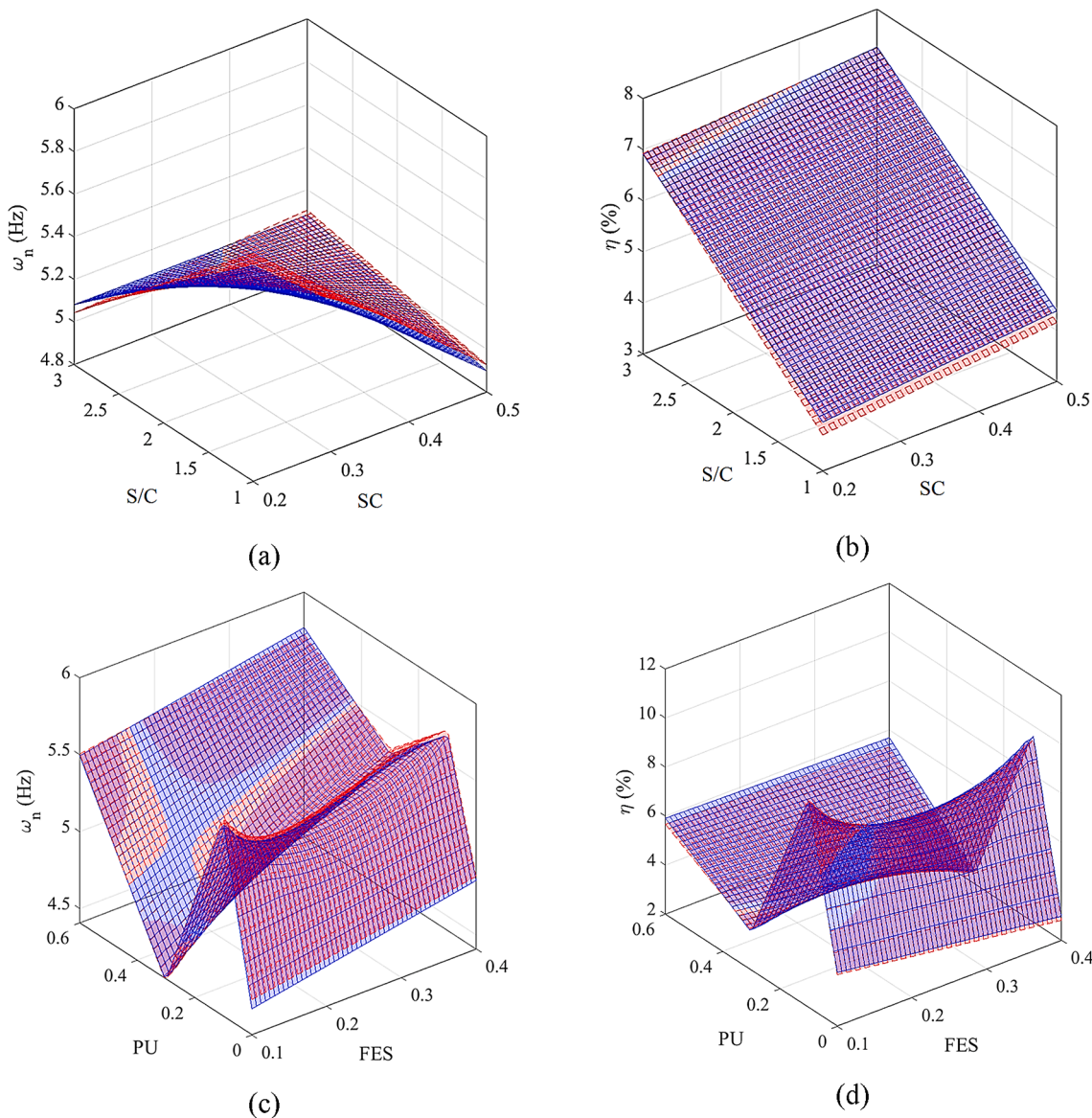


Fig. 16. ANN graphical results of (a) Natural Frequency (ω_n) by SC and S/C, (b) damping (η) by SC and S/C, (c) Natural Frequency (ω_n) by PU and FES (d) damping (η) by PU and FES. (Legend: ■ Real, ■ ANN predicted).

to one (0.99723), indicating that the observed ANN data are reliable and accurate in representing the behavior of the MPUFES modal model. The overall training results are shown in Fig. 15a, with the best training performance measured by the MSE obtained at the eighth interaction (Epoch 8). This demonstrates that the ANN has a fast convergence that helps reduce training time. In Fig. 15b, the error histogram describes the difference between the target value and value after training the neural net. The better the neural net is trained, the more concentrated the histogram gets near zero.

(Intentionally left blank).

Finally, Fig. 16 shows the prediction results of the ANN compared to the test data (not known by the ANN model) in graphical form. Test data is information that has not been used in network training. This test is the most effective approach to determine whether or not the network has been properly taught because they are unknown. The results showed that the net performed as expected. It is clear that, particularly in the circumstances of damping and natural frequency, the net response follows the same pattern as the real response. The net displayed low errors even for the extreme values of the variables S/C, SC, FES, and PU.

Plots are performed by pairs of decision variables for graphical

visualization. From the results obtained, complementary to Fig. 14, it is possible to infer about some aspects: i) The natural frequency has low variation as a function of the sand/cement and coarse sand rate and is more sensitive to the presence of PU (Fig. 17(c)); ii) the second modal response, damping, presents a linear behavior as a function of the sand/cement and coarse sand ratio. A sand/cement ratio ~ 3 with high coarse sand ratios contribute to an increase in structural damping. Considering the parameters of PU and foundry sand, the same pattern is observed for the damping as observed for the natural frequency. The PU variable introduced nonlinearities in the system.

(Intentionally left blank).

In this sense, the results of the neural network were satisfactory. Due to the difficulty in performing a high number of physical tests, the network was able to reproduce an adequate response pattern.

The results found for trained ANN and the results of the full factorial model regression (FFD) following the Design of Experiments (DOE) demonstrate that ANN can be used to predict the dynamic behavior of cementitious mortars with polyurethane powder residues and sand residues from exhaust casting.. In addition, the artificial neural networks presented a substantial performance for the tested (unknown) data:

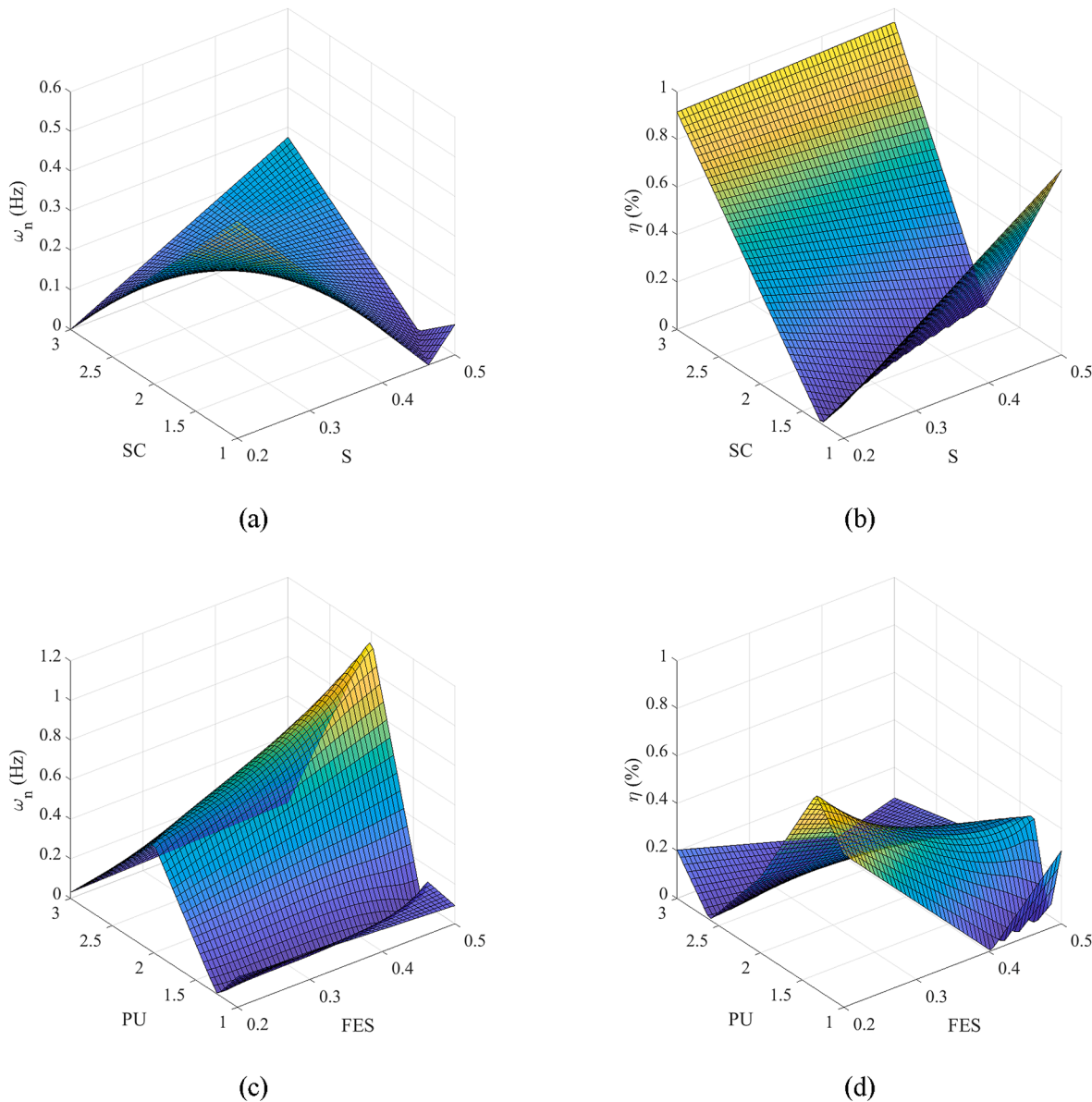


Fig. 17. The difference of the predicted the real data with performance of 1.3909.

performance of 1.39 and the new Fig. 17 highlight the difference of predicted and real data. It can be seen that the error was substantially small and not uniform. There are some regions, especially in the bounds, where the error presented higher values.

The authors reached significant results using analysis parameters to investigate the response to deformation in engineering structures, an approach similar to those adopted in this study [46,47;48]. Once the linear regression models and ANN were compared to evaluate the accuracy of the parameters.

5. Conclusions

The modal response of mortar mixtures with polyurethane incorporation and used foundation sand was examined experimentally to determine the effects of design factors. During the free vibration testing, which isolated the effect of PU, the natural frequency of MPUFES changed from increasing by 11.6 % to decreasing by -21.7 %. While under the influence of FES alone, the natural frequency varied with an increase of 1.8 % and a drop of -4.0 %.

The damping factor testing revealed a pattern resembling the natural

frequency with more fluctuation. If you focus on the impact of PU alone, you can see variety with increases of 78.7 % and decreases of -47.3 %. When the impact of FES is taken out, variation with increases of 26.0 % and decreases of -2.2 % can be seen.

Additionally, the experimental data when compared to the statistical findings revealed that the MPUFES design variables significantly influenced the rise and fall of the modal characteristics, natural frequency, and damping factor of the waste-filled mortars in comparison to the waste-free mortars. Furthermore, the ANN demonstrated outstanding modal response prediction performance with the experimental tests run in this inquiry. This ANN was trained using a subset of the experimental data set.

To better understand the impacts and behavior of these wastes on the modal response of reinforced mortars, additional analysis and testing are needed. Additional research on free and forced vibration using this method, the design characteristics of those tested, and the production of the mortars utilized and selected in this study may aid in elucidating the mechanisms leading to the results attained.

As a result, it was shown that, the modal or dynamic analysis of mortar with polyurethane waste and foundry sand from exhaust can be

predicted using an ANN model with a not too large number of samples (108 samples) with small errors. This study contributes to experimental work in the form of mapping mixture proportions and by the variations of modal parameters such as natural frequency and loss factor. Numerically, this can be achieved without wasting material, thus reducing design costs. In conclusion, RNNs are robust and a viable tool with potential to predict cementitious mortar properties.

CRediT authorship contribution statement

Lucas Ramon Roque da Silva: Conceptualization, Methodology, Writing – original draft. **Flávio Cirino Gaspar:** Investigation. **Paulo Cesar Gonçalves:** Visualization. **Valquíria Claret dos Santos:** Data curation. **Mirian de Lourdes Noronha Motta Melo:** Supervision. **Guilherme Ferreira Gomes:** Software, Validation, Writing – review & editing.

Declaration of Competing Interest

The authors declare that they have no known competing financial interests or personal relationships that could have appeared to influence the work reported in this paper.

Data availability

No data was used for the research described in the article.

Acknowledgements

The authors would like to acknowledge the financial support from the Brazilian agency CNPq (Conselho Nacional de Desenvolvimento Científico e Tecnológico), CAPES (Coordenação de Aperfeiçoamento de Pessoal de Nível Superior), FAPEMIG (Fundação de Amparo à Pesquisa do Estado de Minas Gerais - APQ-00385-18), MAHLE Metal Leve S.A and Indústria e Comércio Fox de Reciclagem Economia Circular Ltda.

References

- [1] Abdolpour H, Garzón-Roca J, Escusa G, Sena-Cruz JM, Barros JAO, Valente IB. Composite modular floor prototype for emergency housing applications: Experimental and analytical approach. *J Compos Mater*, SAGE Publications Ltd 2018;52(13):1747–64.
- [2] ABNT NBR 13276. (2016). “Mortars applied on walls and ceilings - Determination of the consistency index”, ABNT/CB-018 Cimento, Concreto e Agregados.
- [3] ABNT NBR 16697. (2008). “Portland cement -Requirements”, ABNT/CB-018 Cimento, Concreto e Agregados.
- [4] Nbr ABNT, 248.. Aggregates - Sieve analysis of fine and coarse aggregates. ABNT/CB-018 Cimento, Concreto e Agregados 2003.
- [5] ABNT NBR 7175. (2003). “Hydrated lime for mortars - Requirements”.
- [6] ABNT NBR 9778. (2009). “Hardened mortar and concrete - Determination of absorption, voids and specific gravity”, ABNT/CB-018 Cimento, Concreto e Agregados.
- [7] Apostolopoulou M, Armaghani DJ, Bakolas A, Douvika MG, Moropoulou A, Asteris PG. Compressive strength of natural hydraulic lime mortars using soft computing techniques. *Procedia Struct Integrity* 2019;17:914–23.
- [8] Asteris PG, Apostolopoulou M, Skentou AD, Moropoulou A. Application of artificial neural networks for the prediction of the compressive strength of cement-based mortars. *Comput Concrete* 2019;24(4):329–45.
- [9] Astm c494-m-19.. Standard Specification for Chemical Admixtures for Concrete. ICS Code 2020-91(100):30.
- [10] Bala, A. and Gupta, S. (2021), “Thermal resistivity, sound absorption and vibration damping of concrete composite doped with waste tire Rubber: A review”, *Construction and Building Materials*, Vol. 299, available at: <https://doi.org/10.1016/j.conbuildmat.2021.123939>.
- [11] Bottega WJ. Engineering Vibrations. In: Group T, editor. & F. 2nd ed. New York: CRC Press; 2006.
- [12] Briones-Llorente R, Barbosa R, Almeida M, Montero García EA, Rodríguez Saiz Á, García EAM, et al. Ecological design of new efficient energy-performance construction materials with rigid polyurethane foam waste. *Polymers*, MDPI AG 2020;12(5):1048.
- [13] Buscema M. Back Propagation Neural Networks. *Subst Use Misuse* 1998;33(2): 233–70.
- [14] Chong EK, Zak SH. An Introduction to Optimization. 2004.
- [15] Clarence W. de Silva. (2007), *Vibration Damping, Control, and Design*, 1st Editio., Boca Raton.
- [16] Ding X, Chen Z, Xu M. Shaking table experiment of a recycled concrete block masonry building structure with a ‘self-contained’ structural system. *Adv Struct Eng* 2021;24(3):422–36.
- [17] Diniz CA, Cunha SS, Gomes GF, Ancelotti AC. Optimization of the layers of composite materials from neural networks with Tsai-Wu Failure Criterion. *J Fail Anal Prev* 2019;19(3):709–15.
- [18] Duarte APC, Silva BA, Silvestre N, de Brito J, Júlio E, Castro JM. Finite element modelling of short steel tubes filled with rubberized concrete. *Compos Struct* 2016; 150:28–40.
- [19] Eldin NN, Senouci AB. Rubber-tire particles as concrete aggregate. *J Mater Civ Eng* 1993;5(4):478–96.
- [20] Gao H, Sun Q. Study on Fatigue Test and Life Prediction of Polyurethane Cement Composite (PUC) under High or Low Temperature Conditions. *Adv Mater Sci Eng* 2020;1–14.
- [21] Haykin S. *Neural Networks. A Comprehensive Foundation*. 1994.
- [22] Heitz T, Giry C, Richard B, Raguenau F. Identification of an equivalent viscous damping function depending on engineering demand parameters. *Eng Struct* 2019; 188:637–49.
- [23] Hou L, Xu R, Chen D, Xu S, Aslani F. Seismic behavior of reinforced engineered cementitious composite members and reinforced concrete/engineered cementitious composite members: a review. *Struct Concrete* 2020;21(1):199–219.
- [24] Industrias Fox. (2020), “Indústria e Comércio Fox de Reciclagem Economia Circular Ltda.”, available at: <https://www.industriafox.com.br/>.
- [25] ISO 13320. (2020), “Particle size analysis — Laser diffraction methods”, ISO/TC 24/SC 4 Particle characterization.
- [26] He J, Fu Z-F. *Modal Analysis*. 2004.
- [27] Khatib ZK, Bayomy FM. Rubberized Portland Cement Concrete. *J Mater Civ Eng* 1999;11(3):206–13.
- [28] Khatir S, Tiachacht S, Le Thanh C, Ghadourah E, Mirjalili S, Abdel Wahab M. An improved Artificial Neural Network using Arithmetic Optimization Algorithm for damage assessment in FGM composite plates. *Compos Struct* 2021;273:114287.
- [29] Khodadadi, N. and Mirjalili, S. (2022), “Truss optimization with natural frequency constraints using generalized normal distribution optimization”, *Applied Intelligence*, available at:<https://doi.org/10.1007/s10489-021-03051-5>.
- [30] Kovács, Z.L. (2002), *Redes Neurais Artificiais*, edited by Editora Livraria da Física.
- [31] Kwon S, Ahn S, Koh H-I, Park J. Polymer concrete periodic meta-structure to enhance damping for vibration reduction. *Compos Struct* 2019;215:385–90.
- [32] Lee KS, Choi J-I, Park SE, Hwang J-S, Lee BY. Damping property of prepacked concrete incorporating coarse aggregates coated with polyurethane. *Cem Concr Compos*, Elsevier Ltd 2019;93:301–8.
- [33] Li, T. and Singh, A. (2021), “Influence of crack on the damping properties of recycled concrete”, *Construction and Building Materials*, Vol. 311, available at: <https://doi.org/10.1016/j.conbuildmat.2021.125324>.
- [34] Li T, Xiao J, Sui T, Liang C, Li L. Effect of recycled coarse aggregate to damping variation of concrete. *Constr Build Mater* 2018;178:445–52.
- [35] Liang, C., Fu, Y., Wang, C., Gao, Y. and Zhao, J. (2022), “Damping of rubberized recycled aggregate concrete and damping estimation of its elements by finite element analysis”, *Composite Structures*, Vol. 281, available at: <https://doi.org/10.1016/j.compstruct.2021.114967>.
- [36] Liang C, Liu T, Xiao J, Zou D, Yang Q. Effect of Stress Amplitude on the Damping of Recycled Aggregate Concrete. *Materials* 2015;8(8):5298–312.
- [37] Liang C, Xiao J, Wang Y, Wang C, Mei S. Relationship between internal viscous damping and stiffness of concrete material and structure. *Structural Concrete* 2021; 22(3):1410–28.
- [38] Liu K, Yan J, Zou C. A pilot experimental study on seismic behavior of recycled aggregate concrete columns after freeze-thaw cycles. *Constr Build Mater* 2018;164: 497–507.
- [39] Lyne C, C. (2019), “AN ARTIFICIAL NEURAL NETWORK MODEL FOR THE CORROSION CURRENT DENSITY OF STEEL IN MORTAR MIXED WITH SEA WATER”, *International Journal of GEOMATE*, Vol. 16 No. 56, available at: <https://doi.org/10.21660/2019.56.4585>.
- [40] Ma H, Dong J, Liu Y, Yang D. Cyclic loading tests and shear strength of composite joints with steel-reinforced recycled concrete columns and steel beams. *Eng Struct* 2019;199:109605.
- [41] Ma H, Xue J, Zhang X, Luo D. Seismic performance of steel-reinforced recycled concrete columns under low cyclic loads. *Constr Build Mater* 2013;48:229–37.
- [42] Ma Y, Zhang K, Deng Z. Wave component solutions of free vibration and mode damping loss factor of finite length periodic beam structure with damping material. *Compos Struct* 2018;201:740–6.
- [43] Martins, M.A. de B., da Silva, L.R.R., Ranieri, M.G.A., Barros, R.M., dos Santos, V. C., Gonçalves, P.C., Rodrigues, M.R.B., et al. (2021), “Physical and Chemical Properties of Waste Foundry Exhaust Sand for Use in Self-Compacting Concrete”, *Materials*, Vol. 14 No. 19, p. 5629.
- [44] Mei S, Su L, Li P, Wang Y. Material Damping of Concrete under Cyclic Axial Compression. *J Mater Civ Eng* 2018;30(3):04017295.
- [45] Montgomery DC. *Design and Analysis of Experiments*. John Wiley & Sons; 2017.
- [46] Moslemi N, Abdi B, Gohari S, Sudin I, Atashpaz-Gargari E, Redzuan N, et al. Thermal response analysis and parameter prediction of additively manufactured polymers. *Appl Therm Eng* 2022;212:118533.
- [47] Moslemi N, Abdi B, Gohari S, Sudin I, Redzuan N, Ayob A, et al. Influence of welding sequences on induced residual stress and distortion in pipes. *Constr Build Mater* 2022;342:127995.

- [48] Moslemi N, Gohari S, Abdi B, Sudin I, Ghandvar H, Redzuan N, et al. A novel systematic numerical approach on determination of heat source parameters in welding process. *J Mater Res Technol* 2022;18:4427–44.
- [49] Moustafa A, ElGawady MA. Mechanical properties of high strength concrete with scrap tire rubber. *Constr Build Mater* 2015;93:249–56.
- [50] Naga Rajesh K, Rath MK, Markandeya Raju P. A research on sustainable micro-concrete. *Int J Recent Technolo Eng* 2019;8 No. 2 Special:1137–9.
- [51] Naik TR, Patel VM, Parikh DM, Tharaniyil MP. Utilization of Used Foundry Sand in Concrete. *J Mater Civ Eng* 1994;6(2):254–63.
- [52] Nunes K, Maher C. Comparison of construction and demolition waste management between Brazil, European Union and USA. *Waste Manage Res: The J Sustainable Circular Economy* 2020;38(4):415–22.
- [53] Onyari EK, Iketun BD. Prediction of compressive and flexural strengths of a modified zeolite additive mortar using artificial neural network. *Constr Build Mater* 2018;187:1232–41.
- [54] Avitable P. Modal Testing: a practitioner's Guide. John Wiley; 2018.
- [55] Parashar A, Aggarwal P, Saini B, Aggarwal Y, Bishnoi S. Study on performance enhancement of self-compacting concrete incorporating waste foundry sand. *Constr Build Mater* 2020;251:118875.
- [56] Pramanik A. Problems and solutions in machining of titanium alloys. *The Int J Adv Manuf Technol* 2014;70(5–8):919–28.
- [57] Clough RW, Penzien J. Dynamics of Structures. (2th Editi. 2003.
- [58] Raffoul S, Garcia R, Pilakoutas K, Guadagnini M, Medina NF. Optimisation of rubberised concrete with high rubber content: An experimental investigation. *Constr Build Mater* 2016;124:391–404.
- [59] Rajasekaran S. Structural Dynamics of Earthquake Engineering - Theory and Application Using MATHEMATICA and MATLAB. Woodhead Publishing; 2012.
- [60] Ribeiro Junior RF, de Almeida FA, Gomes GF. Fault classification in three-phase motors based on vibration signal analysis and artificial neural networks. *Neural Comput Appl* 2020;32(18):15171–89.
- [61] Rao SS, P.g.. Mechanical Vibrations. Pearson, H; 2018.
- [62] Santamaría Vicario I, Alameda Cuenca-Romero L, Gutiérrez González S, Calderón Carpintero V, Rodríguez Saiz Á, Vicario IS, et al. Design and characterization of gypsum mortars dosed with polyurethane foam waste PFW. *Materials*, MDPI AG 2020;13(7):1497.
- [63] Sharma, P. and Gupta, T. (2022), "Comparative Investigation on Mode Shapes and Natural Frequency of Low-Rise RC Frame Building", pp. 885–898.
- [64] Singh G, Siddique R. Effect of waste foundry sand (WFS) as partial replacement of sand on the strength, ultrasonic pulse velocity and permeability of concrete. *Constr Build Mater* 2012;26(1):416–22.
- [65] Singh G, Siddique R. Abrasion resistance and strength properties of concrete containing waste foundry sand (WFS). *Constr Build Mater* 2012;28(1):421–6.
- [66] Souza, C. dos S., Antunes, M.L.P., Valentina, L.V.O.D., Rangel, E.C. and da Cruz, N. C. (2019), "Use of waste foundry sand (WFS) to produce protective coatings on aluminum alloy by plasma electrolytic oxidation", *Journal of Cleaner Production*, Vol. 222, pp. 584–592.
- [67] Spence SMJ, Kareem A. Tall buildings and damping: a concept-based data-driven model. *J Struct Eng* 2014;140(5):04014005.
- [68] Su H, Yang J, Ling T-C, Ghataora GS, Dirar S. Properties of concrete prepared with waste tyre rubber particles of uniform and varying sizes. *J Cleaner Prod* 2015;91: 288–96.
- [69] Suda K, Satake N, Ono J, Sasaki A. Damping properties of buildings in Japan. *J Wind Eng Ind Aerodyn* 1996;59(2–3):383–92.
- [70] Svozil D, Kvasnicka V, Pospichal J. Introduction to multi-layer feed-forward neural networks. *Chemometrics and Intelligent Laboratory Systems* 1997;39(1):43–62.
- [71] Swamy N, Rigby G. Dynamic properties of hardened paste, mortar and concrete. *Matériaux et Constructions* 1971;4(1):13–40.
- [72] Topcu IB. The properties of rubberized concretes. *Cem Concr Res* 1995;25(2): 304–10.
- [73] Torres A, Bartlett L, Pilgrim C. Effect of foundry waste on the mechanical properties of Portland Cement Concrete. *Constr Build Mater* 2017;135:674–81.
- [74] Wang C, Xiao J. Shaking table tests on a recycled concrete block masonry building. *Adv Struct Eng* 2012;15(10):1843–60.
- [75] Wang C, Xiao J, Wang C, Zhang C. Nonlinear damping and nonlinear responses of recycled aggregate concrete frames under earthquake loading. *Eng Struct* 2019; 201:109575.
- [76] Wang C, Xiao J, Zhang C, Xiao X. Structural health monitoring and performance analysis of a 12-story recycled aggregate concrete structure. *Eng Struct* 2020;205: 110102.
- [77] Xue J, Shinozuka M. Rubberized concrete: a green structural material with enhanced energy-dissipation capability. *Constr Build Mater* 2013;42:196–204.
- [78] Yan S, Zou X, Ilkhani M, Jones A. An efficient multiscale surrogate modelling framework for composite materials considering progressive damage based on artificial neural networks. *Compos B Eng* 2020;194:108014.
- [79] You SH, Lee JH, Oh SH. A study on cutting characteristics in turning operations of titanium alloy used in automobile. *Int J Precis Eng Manuf* 2019;20(2):209–16.
- [80] Youssif O, ElGawady MA, Mills JE. Experimental investigation of crumb rubber concrete columns under seismic loading. *Structures* 2015;3:13–27.
- [81] Zhang P, Wang Y, Mei S, Liu B, Xiao J. Nonlinear damping properties of recycled aggregate concrete short columns under cyclic uniaxial compression. *Constr Build Mater* 2020;246:118445.
- [82] Zhang Y, Li B, Li Z, Ma G, Liu Y. Seismic performance of interior beam-column joints in reinforced glazed hollow bead insulation concrete frames. *Eng Struct* 2021;228:111494.
- [83] Zheng L, Sharon Huo X, Yuan Y. Experimental investigation on dynamic properties of rubberized concrete. *Constr Build Mater* 2008;22(5):939–47.
- [84] Zonzini F, Zaulli M, Mangia M, Testoni N, De Marchi L. "HW-Oriented Compressed Sensing for Operational Modal Analysis: the impact of noise in MEMS Accelerometer Networks", *2021 IEEE Sensors Applications Symposium (SAS)*. IEEE 2021:1–5.